UNIVERSITY OF CALIFORNIA, SAN DEIGO

Unraveling the Biological Role and Emerging Capabilities of a Novel Class of Type 2 Diabetes Drug Targets

A Dissertation submitted in partial satisfaction of the

requirements for the degree of Doctor of Philosophy

in

Chemistry

by

John A. Zuris

Committee in Charge:

Professor Patricia A. Jennings, Chair
Professor Joshua S. Figueroa
Professor Gourisankar Ghosh
Professor Clifford P. Kubiak
Professor Jose N. Onuchic
Professor Stanley J. Opella

2012

The Dissertation of John A. Zuris is approved, and it is acceptable in quality and form for publication on microfilm and electronically:

Chair

University of California, San Diego
2012

DEDICATION

I would like to dedicate this work to all the people who have mentored me as well as all those who have provided emotional support in my pursuit of this degree. I want to especially thank Yekaterina Tarasova for her strong love and support.

TABLE OF CONTENTS

LIST OF ABBREVIATIONS

a-Fd	apo-Ferredoxin
CISD	CDGSH iron sulfur domain-containing
DFO	desferrioxamine
DT	Na-Dithionite
DTT	Dithiothreitol
EPR	electron paramagnetic resonance
E. coli	Escherichia coli
E_{acid}	Point at which redox potential is pH independent
E_M	midpoint/redox potential
$E_{M,7}$	midpoint/redox potential at pH 7.0
EDTA	ethylene diamine tetraacetic acid
FeS	iron sulfur
FHQ	$FeCl_3$-8-hydroxyquinoline
GLRX5	Glutaredoxin 5
HBS	HEPES buffered saline
HEK	human embryonic kidney
HSQC	heteronuclear single quantum coherence
IPTG	Isopropyl b-D-1-thiogalactopyranoside
LB	Luria Broth
LDAO	lauryldimethylamine oxide
MM	minimal media
mNT	mitoNEET

NADH	reduced nicotinamide dinucleotide
NADPH	reduced nicotinamide adenine dinucleotide phosphate
NMR	nuclear magnetic resonance
OMM	outer mitochondrial membrane
PAGE	poly-acrylamide gel electrophoresis
PCR	polymerase chain reaction
PDB	protein data bank
pK_{ox}	pH where titrating residue is half-protonated upon reduction
pK_{red}	pH where titrating residue is no longer protonated upon reduction
PPARγ	peroxisome proliferater-activated receptor γ
ROS	reactive oxygen species
RPA	rhodamine B-[(1,10- phenanthrolin-5-yl) aminocarbonyl] benzyl ester
SHE	standard hydrogen electrode
TZD	thiazolidinedione
WFS	Wolfram's Syndrome
WT	wild type
XLSA/A	X-linked sideroblastic anemia with ataxia

LIST OF FIGURES

LIST OF TABLES

ACKNOWELEDGEMENTS

This experience has been so rewarding in so many ways. I would like to thank my advisor, Professor Patricia Jennings, for inspiring me to be a great scientist. I feel very privileged to have had so much time with her writing papers and discussing my project. I understand this is unusual for a graduate student and I really feel lucky to have had her as my boss. I would like to thank my committee for their insightfulness and guidance throughout my graduate career. They are an exceptional group of individuals and I am grateful for the expertise that they all brought to this project.

I would like to thank all the current and past members of the Jennings lab including Melinda Roy, Dr. Andrea Conlan, Dr. Kendra Hailey, Dr. Ben Andrews, Dr. Dominique Capraro, Dr. Jamie Mills, Michael Jamros, Elizabeth Baxter, Sulyman Barkho, Danny Halim, Kaitlin Fisher, Colin Lipper, and David Burban for all of their support. I want to also thank my undergraduates: Charles Wang, Brandon Wong, Pamela Chew, Syed Ali, Howard Yeh, Tung Nguyen, Danny Halim, Michelle Kong, and Alex Navarro. They have all have been exceptional and not only saved me a lot of time with experiments but also solved many challenging problems when I myself was stuck. I know many of them will go on to have great careers in science. Thank you guys!

I would like to thank all of our collaborators. I am thrilled to have had a chance to work with so many amazing people. I'd like to thank Dr. Mark Paddock, Dr. Ed Abresch, and Charlene Chang in the Physics department. I'd also like to thank Professor Rachel Nechushtai of the Hebrew University of Jerusalem. She has been a great collaborator and a great friend. I would also like to thank Professor Zvi Ioav Cabantchik at the Hebrew University of Jerusalem and Professor Ron Mittler at the University of Texas who

collaborator with us on the biological side of the “mNT project”. Lastly, I would like to thank Professor Sean Elliott and his student Daniel Bak of Boston University for their expertise in protein-film voltammetry and providing the first redox data for the mNT project.

Finally, I would like to thank my friends and family for all of their love and support. My friends Johnny, Beau, and Stuart have helped shape me into who I am today and I trust them more than anyone. My uncle Rick has been an amazing scientific mentor for me throughout my college years and has set a standard for me that I still hope to achieve. I want to thank my aunt Suzanne for being the best cheerleader I could imagine. She always has something positive to say and she is an extremely generous person. Most of all I want to thank my best friend, Yekaterina Tarasova. She has been my best friend throughout this journey, and I cannot thank her enough.

Chapter 2, in part, is a reprint of the material as it appears in Biochemistry by Bak DW, Zuris JA, Paddock ML, Jennings PA, Elliott SJ. 48 2009. The dissertation/thesis author was a contributing investigator and contributing author in this paper.

Chapter 3, in part, is a reprint of the material as it appears in Journal of the American Chemical Society by Zuris JA, Halim DA, Conlan AR, Abresch EC, Nechushtai R, Paddock ML, Jennings PA. 132 2010. The dissertation/thesis author was the primary investigator and author of this paper.

Chapter 4, in part, is a reprint of the material that appears in Proceedings of the National Academy of Sciences by Zuris JA, Harir Y, Conlan AR, Shvartsman M, Michaeli D, Tamir S, Paddock ML, Onuchic JN, Mittler R, Cabantchik Z-I, Jennings PA, Nechushtai R. 108 2011. The dissertation/thesis author was the primary investigator and

author of this paper.

Chapter 5, in part, is a reprint of the material as it appears in the Journal of Biological Chemistry by Zuris JA, Ali SS, Yeh H, Nguyen TA, Nechushtai R, Paddock ML, Jennings PA. 287 2012. The dissertation/thesis author was the primary investigator and author of this paper.

VITA

2007	B.S., Biochemistry University of California, Santa Cruz
2009	M.S., Chemistry University of California, San Diego
2009-2012	Research Assistant, University of California, San Diego
2012	Ph.D., Chemistry, University of California, San Diego

Publications

1. Nechushtai R, Conlan AR, Harir Y, Song L, Yogev O, Eisenberg-Domovich Y, Livnah O, Michaeli D, Rosen R, Ma V, Luo Y, **Zuris JA**, Paddock ML, Zvi Ioav Cabantchik ZI, Jennings PA, Mittler R. Characterization of Arabidopsis NEET Reveals an Ancient Role for NEET Proteins in Iron Metabolism. *The Plant Cell*. **2012** [Epub ahead of print]

2. **Zuris JA,** Ali SS, Yeh H, Nguyen TA, Nechushtai R, Paddock ML, Jennings PA. NADPH inhibits [2Fe-2S] cluster transfer from the diabetes drug target mNT to an apo-acceptor protein. *J Biol Chem.* **2012** Apr 6; 287(15):11649-55.

3. **Zuris JA,** Harir Y, Conlan AR, Shvartsman M, Michaeli D, Tamir S, Paddock ML, Onuchic JN, Mittler R, Cabantchik Z-I, Jennings PA, Nechushtai R. Facile transfer of [2Fe-2S] clusters from the diabetes drug target mNT to an apo-acceptor protein. *Proc Natl Acad Sci USA* **2011** Aug 9; 108(32):13047-52.

4. Conlan AR, Paddock ML, Homer C, Axelrod HL, Cohen AE, Abresch EC, **Zuris JA,** Nechushtai R, Jennings PA. Mutation of the His ligand in mNT stabilizes the 2Fe-2S cluster despite conformational heterogeneity in the ligand environment. *Acta Crystallogr D Biol Crystallogr*. **2011** Jun; 67 (Pt 6):516-23.

5. Nechushtai R, Lammert H, Michaeli D, Eisenberg-Domovich Y, **Zuris JA,** Luca MA, Capraro DT, Fish A, Shimshon O, Roy M, Schug A, Whitford PC, Livnah O, Onuchic JN, Jennings PA. Allostery in the ferredoxin protein motif does not involve a conformational switch. *Proc Natl Acad Sci USA*. **2011** Feb 8; 108(6):2240-5.

6. **Zuris JA**, Halim DA, Conlan AR, Abresch EC, Nechushtai R, Paddock ML, Jennings PA. Engineering the redox potential over a wide range within a new class of FeS proteins. *J Am Chem Soc.* **2010** Sep 29;132(38):13120-2.

7. Bak DW, **Zuris JA,** Paddock ML, Jennings PA, Elliott SJ. Redox characterization of the FeS protein MNT and impact of thiazolidinedione drug binding. *Biochemistry.* **2009** Nov 3; 48(43):10193-5.

8. Conlan AR, Axelrod HL, Cohen AE, Abresch EC, **Zuris JA,** Yee D, Nechushtai R, Jennings PA, Paddock ML. Crystal structure of Miner1: The redox-active 2Fe-2S protein causative in Wolfram Syndrome 2. *J Mol Biol.* **2009** Sep 11; 392(1):143-53.

Honors

Heme and Blood Proteins Training Grant	2008-2011
Bruno Zimm Award for outstanding thesis in Biophysics	2012

ABSTRACT OF DISSERTATION

Unraveling the Biological Role and Emerging Capabilities of a Novel Class of Type 2 Diabetes Drug Targets

by

John A. Zuris

Doctor of Philosophy in Chemistry

University of California, San Diego, 2012

Professor Patricia A. Jennings, Chair

MitoNEET (mNT) is an outer mitochondrial membrane iron-sulfur (FeS) protein and a target of the thiazolidinedione (TZD) class of anti-diabetes drugs. The [2Fe-2S] cluster in mNT is ligated by a rare 3-Cys-1-His coordination. As FeS proteins usually function in electron transfer (redox) or in transfer of their clusters to apo-acceptor proteins, we investigated whether the TZDs affect the protein's redox potential ($E_{M,7}$). We found that TZD binding negatively shifts $E_{M,7}$ by ~100 mV, whereas in the cluster-coordinating His87 to Cys mutant (H87C) this effect is not observed. This suggests that His87 is critical to TZD communication with the [2Fe-2S] cluster of mNT.

We further investigated the importance of residues near the cluster and discovered that mNT could tolerate an array of mutations that modified $E_{M,\ 7}$ over a range of ~700 mV. This is the largest range engineered in an FeS protein and, importantly, spans the cellular redox range (+200 to -300 mV). Therefore, mNT is potentially useful for both physiological redox studies and industrial applications as a stable, water-soluble, redox agent.

We investigated whether mNT functions as a cluster transfer protein and if TZDs affect transfer. We observed facile [2Fe-2S] cluster transfer between oxidized mNT and apo-ferredoxin (a-Fd) both in vitro and with a mitochondrial iron detection assay in cells. The H87C mutant inhibits transfer of the [2Fe-2S] clusters both in vitro and in cells. Importantly, TZDs inhibit iron transfer from mNT to mitochondria. This finding is interesting in light of the role of iron overload in diabetes. Finally, we show that NADPH shifts $E_{M,\ 7}$ negatively and inhibits cluster transfer in a manner similar to the TZDs, The most critical cellular function of NADPH is in the maintenance of a pool of reducing equivalents, which is essential to counteract oxidative damage. Taken together, our findings suggest a likely role for mNT in [2Fe-2S] and/or iron transfer to acceptor proteins and support the idea that pioglitazone's anti-diabetic mode of action may, in part, be to inhibit transfer of mNT's [2Fe-2S] cluster and protect cells from iron-overload.

Chapter 1

Introduction

Type 2 diabetes mellitus is a chronic disease that has emerged as an epidemic both here in the United States and abroad, affecting nearly 300 million people (1). This disease is characterized by the presence of high blood glucose levels as a result of insulin resistance (2). In addition, several of the cellular and physiological effects of type 2 diabetes are now classified under the more general term metabolic syndrome (Figure 1-1), which includes oxidative stress, whereby the cell environment is no longer highly reducing, and this phenomenon is also observed in patients diagnosed with type 2 diabetes (3). Many drug treatments have been generated within the last few decades to combat this disease. The most commonly prescribed class of anti-diabetic drugs are known as thiazolidinediones (TZDs) (4, 5). TZDs were developed based upon their ability to bind to peroxisome proliferater-activated receptor γ (PPARγ) (6), a nuclear receptor that when stimulated affects genes involved in lipid and glucose metabolism (7).

Although TZDs were developed based on PPARγ binding, muscle specific PPARγ knockout mice on a high fat diet are TZD responsive (8) indicating that TZDs bind to other targets in the cell. In 2004, studies with ^{3}H-labeled pioglitazone indicated drug binding to crude mitochondrial membranes (9). Photo-affinity labeling studies identified a new mitochondrial target that was identified by a combination of mass spectrometry analysis and amino acid sequencing. The protein, listed in databases only as a protein of unknown function, was named mitoNEET (mNT), for its localization to the mitochondria, and a rare "NEET" portion of its protein sequence (9). Researchers were able to show that this protein specifically interacts with pioglitazone, perhaps in complex with other mitochondrial proteins. The discovery that pioglitazone interacts with mNT, in

concordance with the PPARγ mouse knockout data, suggested that TZDs may have beneficial effects mediated through this mitochondrial target, and that the negative side effects of the TZDs may be due to binding to PPARγ.

The subcellular localization of mNT was confirmed in tissue culture experiments, which showed a co-localization of mNT with the mitochondrion using the mitochondrial labeling dye Mito-Tracker Red (10). When the N-terminal 32 residues were removed from the protein, it was no longer targeted to mitochondria. When these 32 amino acids were tagged to the N-terminus of GFP, however, mitochondrial localization was again observed (10). Though the N-terminus is not a classical mitochondrial target, sequence, this sequence is both necessary and sufficient for correct localization of the mNT. As the N-terminus of the protein contains a predicted membrane spanning sequence, it was postulated that this portion of the protein spans one of the mitochondrial membranes. MNT is specifically located in the outer mitochondrial membrane (OMM), with the soluble domain directed into the cytosol as demonstrated by mitochondrial fractionation and protease sensitivity experiments (10). The protein is encoded by the gene CISD1, (Figure 1-3), and is evolutionarily conserved. The gene exists not only in mammals, but plants and protozoa as well, though it is surprisingly absent in yeast and most bacteria. The mNT protein sequence, while different among species at its N-terminus, has an area of extremely high homology, especially in the annotated “CDGSH” domain. In particular, within the CDGSH domain, a consensus sequence exists given as C-X-C-X2-(S/T)-X3-P-X-C-D-G-(S/A/T)-H. In many plants and unicellular organisms, the CDGSH family is represented by only one gene. However, in many mammals, including humans, mNT is just one of three family members. The other two human proteins, Miner1 and Miner2

(mNT related 1, and 2), are encoded by genes CISD2 and CISD3, respectively (10). It is also noteworthy that this conserved CDGSH domain is predicted to bind a zinc finger. Though mNT was originally annotated as a zinc finger protein, biochemical data indicated that an iron sulfur cluster was bound to the protein (11). Specifically, mNT binds a [2Fe-2S] cluster (11). This cluster is reversibly reducible, and is also pH sensitive; when the pH is lowered, the cluster is released from its protein scaffold (Figure 1-4) (11).

The crystal structure of mNT revealed that the protein is homodimeric, with each monomer binding one [2Fe-2S] cluster (Figure 1-5, left) (12-14). The tertiary and quaternary fold of mNT is novel. The protein is composed of two distinct domains, a Beta-Cap domain, that contains a strand swap between dimers, and a Cluster-Binding domain (Figure 1-5, right). Even more striking was the revelation of the ligands that bound each iron sulfur cluster. In mNT, the cluster is bound by three cysteines and one histidine (12-14). This coordination is extremely rare among all known [2Fe-2S] proteins (15), and within the CDGSH protein family, the ligand residues constitute part of the consensus sequence of the protein (Figure 1-3). These proteins contain the [2Fe-2S] functional cofactor coordinated by residue side chains (Figure 1-5, right). In general, [2Fe-2S] clusters are bound by a combination of cysteine, histidine, aspartic acid, and even serine side chains (16). However, the most common coordination forms are the Rieske-type, in which the iron sulfur cluster is bound by two histidines and two cysteines, and the ferrodoxin-type, bound by four cysteine residues (16). The mNT coordination, therefore, became the first identified hybrid of these two most common ligand combinations, and is a hallmark characteristic of the CDGSH family of proteins.

Interestingly, the sole histidine residue is surprisingly solvent exposed, a feature largely absent amongst the histidines of Rieske proteins, and may be important for the protein's possible redox and/or [2Fe-2S] cluster transfer properties (Figure 1-5).

The importance of iron sulfur cluster proteins in biology is evidenced by their conservation from unicellular organisms to higher level plants and mammals and by their abundance within cells (17, 18). Iron-sulfur proteins participate in basic cellular processes, primarily electron transfer. They also comprise the main working components in iron sulfur cluster biogenesis (Figure 1-6) (17). Iron sulfur proteins participate as biological catalysts for a multitude of reactions, serve as structural scaffolds, and can even function as transcription factors (17, 19, 20). Importantly, iron sulfur cluster proteins can scavenge cellular damaging free radicals, particularly under conditions of oxidative stress. Free iron in the cell can also be toxic, and is therefore highly regulated, often by iron sulfur cluster proteins that can sequester these harmful ions. Because many iron sulfur cluster proteins are critical components in fundamental cellular processes, mis-regulation of these proteins can result in human disease (21-23). Given the fact that mNT was discovered as a potential diabetes drug, it is not surprising that the CDGSH family of proteins is important in regulating cellular health. For example, the human homolog of mNT, Miner1, is important in Wolfram Syndrome 2 (WFS2) (23). Specifically, a single base pair transversion in the coding DNA of the Miner1 CISD2 gene causes a missplicing error, the consequence of which is a dramatically truncated form of the Miner1 protein. Wolfram Syndrome (WFS), although variable in symptomatic output, is characterized by diabetes insipidus, diabetes mellitus, optic atrophy, and deafness, so it is often known as DIDMOAD (24, 25). Similar to mNT

knockouts, Miner1 knockout mice displayed a decrease in mitochondrial oxidative capacity. In addition, cells from the knockout mice have an increased incidence of mitochondrial breakdown in muscle and nerve cells (26). This mitochondrial degradation then resulted in higher rates of cellular autophagy (27). Thus, the CDGSH family members are critical to normal physiological functioning.

Due to the strong evidence shows that the CDGSH family of proteins plays a critical cellular role in mammals, understanding how these proteins function is of critical importance. In order to fully understand this role, the properties of these proteins need to be fully characterized. In this study, a detailed characterization of CDGSH family member mNT is investigated. Using a combination of biophysical and tissue culture techniques, we describe the properties of this family of proteins in the context of its functional cofactor, the [2Fe-2S] cluster. We show that mNT's redox and cluster transfer properties are strongly dependent on the unique 3-Cys-1-His coordination environment of the [2Fe-2S] cluster. Importantly, we show the binding of TZDs dramatically alters both redox and cluster transfer (28, 29). We also show that physiological reducing agent NADPH may interact with mNT in a manner similar to the TZDs (30). Finally, this work reveals that mNT may cause iron overload in mitochondria under conditions of oxidative stress, which is observed in patients with type 2 diabetes (31), and that TZDs alleviate this stress. Taken together, mNT is likely an important cellular target for the TZDs in their therapeutic mode of alleviating type 2 diabetes and the findings of this work may lead to improved drug design for targets that preferentially interact with mNT while possibly avoiding PPARγ.

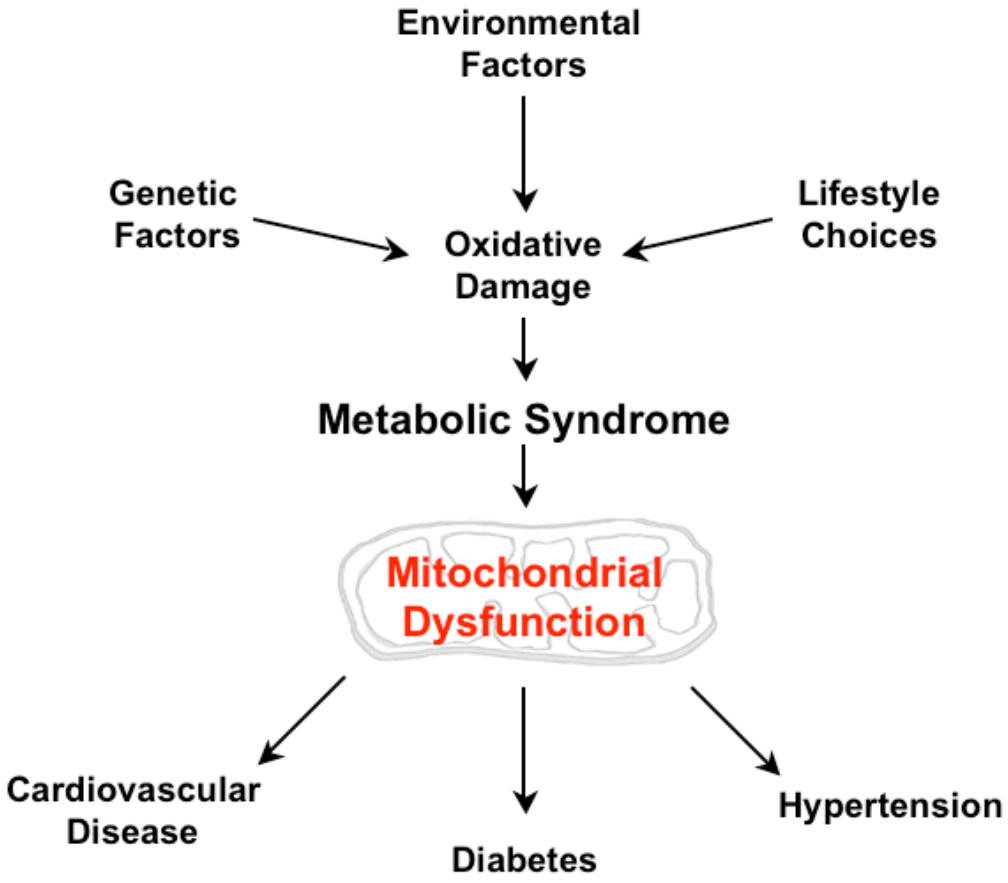

Figure 1-1: Mitochondrial dysfunction is a result of metabolic syndrome. Metabolic syndrome is a result of a host of genetic, environmental, and lifestyle factors that contribute to oxidative stress. The end result of oxidative stress is often diabetes (3).

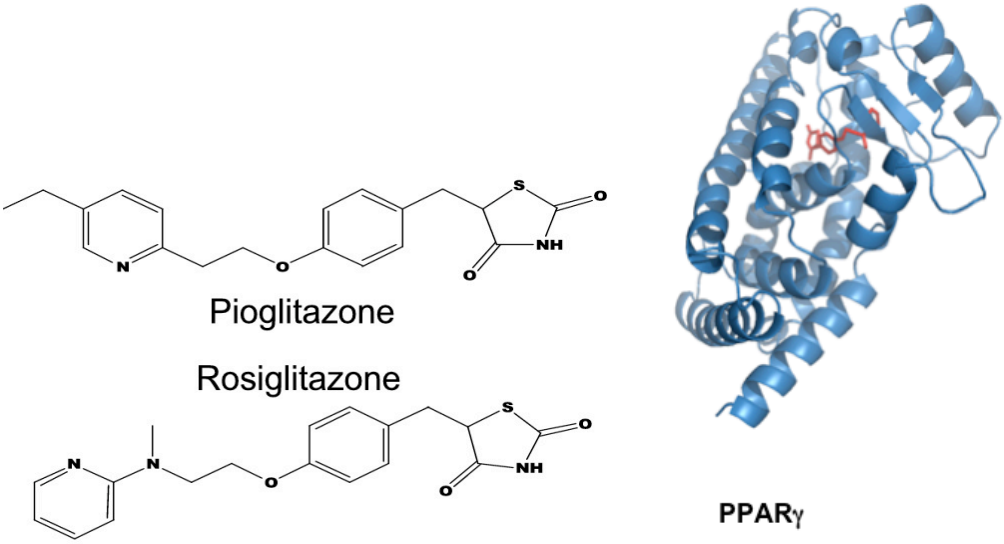

Figure 1-2: The PPARγ-TZD Paradigm. (Left) The thiazolidinedione (TZD) class of anti-type 2 diabetes drugs contains two widely used PPARγ agonists pioglitazone and rosiglitazone (4). (Right) PPARγ is believed to be the TZD target that is responsible for the therapeutic mode of action for the drugs. However, several side effects of the TZDs are known to act via PPARγ whereas several beneficial effects of the TZDs have been shown to be PPARγ–independent (8).

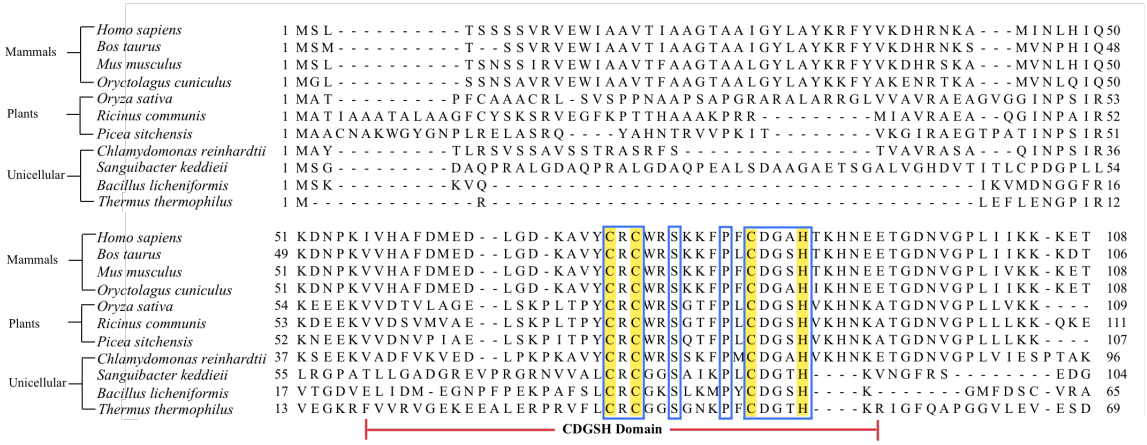

Figure 1-3: Sequence alignment of CDGSH protein family amongst species reveals high area of conservation. When sequences from many organisms, including mammals, plants as well as cyanobacteria and other protozoa are aligned, the area of highest conservation occurs in the "CDGSH domain" (underlined in red). From this area, a consensus sequence arises (boxed in blue), which includes the iron sulfur coordinating ligands, highlighted in yellow.

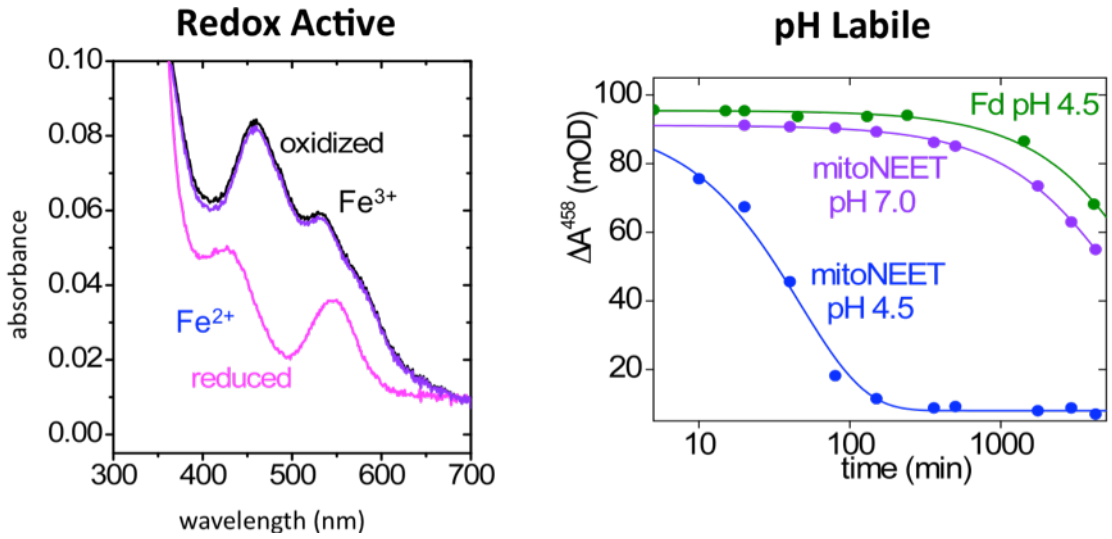

Figure 1-4: The [2Fe-2S] cluster in mNT is redox active and pH labile. Optical spectra of mNT shown as isolated (black), after reduction with dithionite (pink), and after subsequent oxidation with O_2 (purple). The stability of the 2Fe-2S cluster of mNT at pH 7.0 (purple) and 4.5 (blue) when compared with that of ferredoxin (Fd), monitored at 420 nm at pH 4.5 (green) (11).

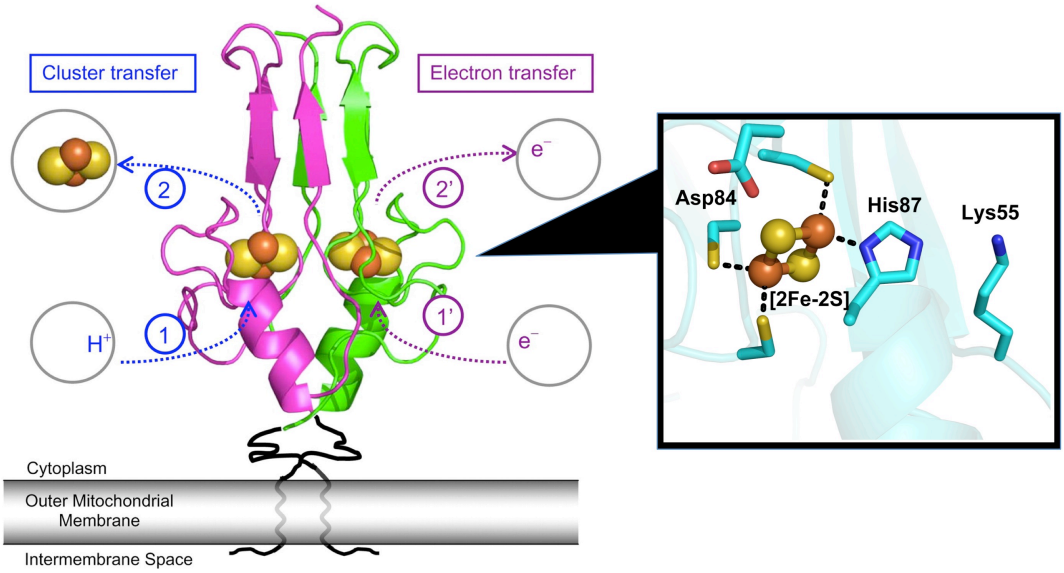

Figure 1-5: The tertiary and quaternary fold of mNT (PDB code 2QH7) is novel. The protein is composed of two distinct domains, a Beta-Cap domain, that contains a strand swap between dimers, and a cluster-binding domain. Interestingly, the sole histidine residue is surprisingly solvent exposed, a feature largely absent amongst the histidines of Rieske proteins, and may be important for the protein's possible redox and/or [2Fe-2S] cluster transfer properties (12).

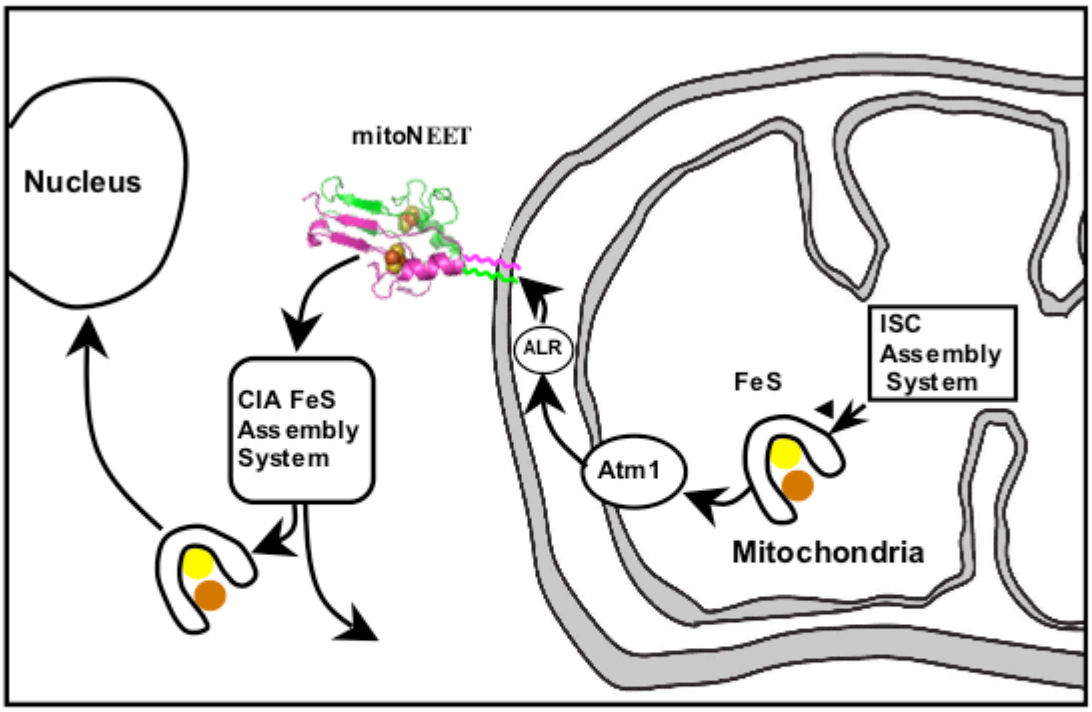

Figure 1-6: Possible role for mNT in FeS cluster trafficking and iron management. The mechanism by which FeS clusters are assembled in the mitochondria and exported to the cytoplasm is an active field of research. Specifically, how FeS clusters are able to pass through the outer-mitochondrial membrane is not well understood (17). This cartoon illustrates the mitochondrial iron sulfur cluster assembly machinery (ISC) and the cytosolic iron sulfur assembly machinery (CIA) in action with mNT as the possible conduit between the two pathways.

Chapter 2

Redox Characterization of the FeS Protein MitoNEET and Impact of Thiazolidinedione Drug Binding

ABSTRACT

MitoNEET (mNT) is a small mitochondrial protein that has been identified recently as a target for the thiazolidinedione (TZD) class of diabetes drugs. mNT also binds a unique three-His-1-Cys-ligated [2Fe-2S] cluster. Here we use protein film voltammetry (PFV) as a means to probe the redox properties of mNT and demonstrate the direct impact of TZD drug binding upon the redox chemistry of the FeS cluster. When TZDs bind, the midpoint potential at pH 7 is lowered by more than 100 mV, shifting from ~0 to -100 mV. In contrast, a His87Cys mutant negates the ability of TZDs to affect the midpoint potential, suggesting a model of drug binding in which His87 is critical to communication with the FeS center of mNT.

INTRODUCTION

While the thiazolidinedione (TZD)1 drugs have been useful in the treatment of type 2 diabetes, their primary mode of action has been attributed to activation of peroxisome proliferator-activated receptor γ (PPARγ) (4). Recent appreciation of PPARγ-independent modes of TZD action (32) spurred the discovery of mNT, a mitochondrial protein, through a cross-linking study with a photoactive form of the TZD drug pioglitazone (Figure 2-1) (9). Intriguingly, mNT bears a [2Fe-2S] cluster (11), and the cardiac mitochondria of mice lacking mNT display dramatic decreases in respiratory function (10). The typical association of FeS proteins with redox events in biology, the growing appreciation of the interplay between mitochondrial dysfunction and type 2 diabetes (33), and the observation of oxidative stress in diabetic patients (31) led us to posit that mNT may possess redox chemistry that is an important component of mitochondrial function, and that TZD drug binding may stabilize normal function of

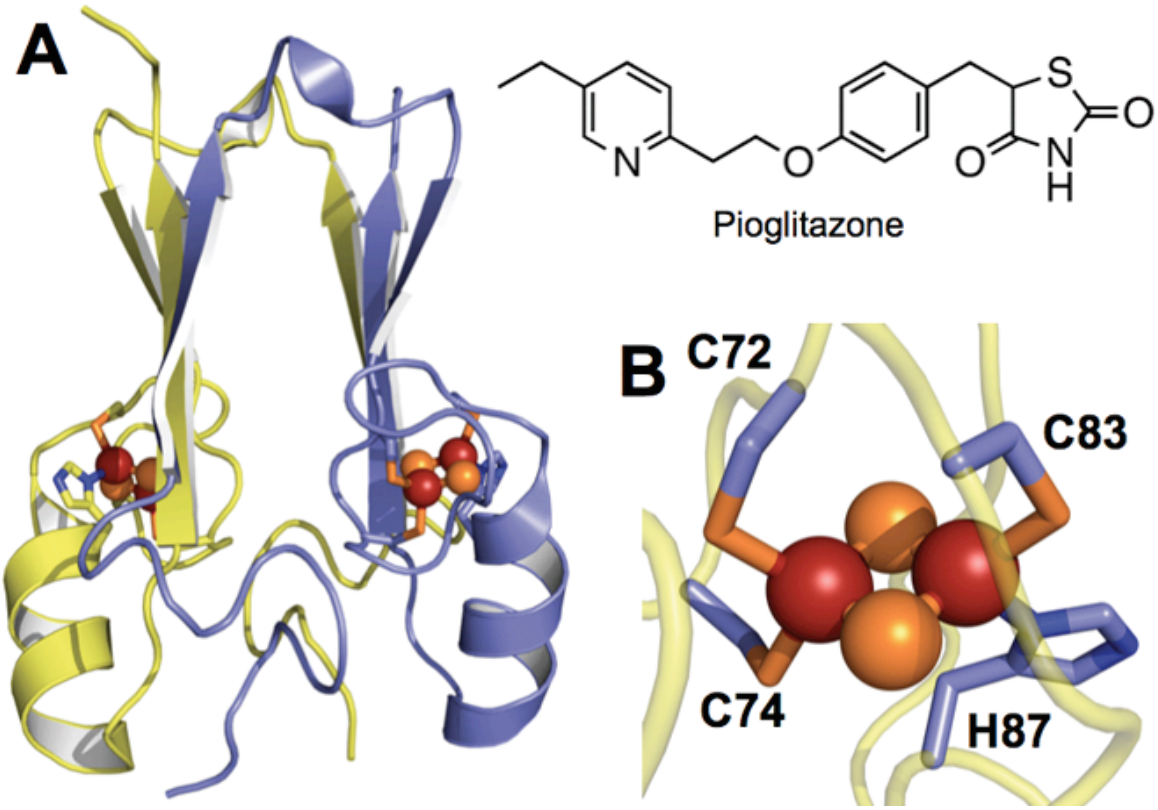

Figure 2-1: mNT cluster binding site and pioglitazone. (A) Overall fold of the mNT soluble domain (PDB entry 2QH7), which interacts with TZD drugs like pioglitazone. (B) Cluster organization, with the inner iron ligated by Cys72 and Cys74 and the outer iron by Cys83 and His87 (28).

mNT in diabetes. Here we describe the redox chemistry of the mNT [2Fe-2S] cluster for the first time, demonstrate that TZD binding directly impacts the mNT reduction potential, and show that TZD binding stabilizes the oxidized state of the wild-type protein. MNT is a small ~17 kDa protein localized to the cytosolic face of the outer mitochondrial membrane by a single transmembrane helix (10). X-ray crystallographic analyses of the soluble portion of the protein (Figure 2-1A) have demonstrated that mNT forms dimers with one [2Fe-2S] cluster per monomer, and a cluster-cluster distance of ~14 Å (12-14). The cluster is uniquely ligated by three Cys residues and one His, a novel coordination environment for [2Fe-2S] clusters (Figure 2-1B), differing from the all-Cys ligation of ferredoxins and the two-Cys, two-His ligation seen in Rieske centers (16). We have used protein film voltammetry (PFV) to interrogate the [2Fe-2S] cluster TZD-free and -bound states of the crystallographically characterized, soluble form of mNT (Figure 2-1A).

RESULTS

Baseline-subtracted oxidative and reductive voltammograms (Figure 2-2B) were averaged to yield midpoint potentials ($E_{M,7}$) over a pH range from 6 to 12 (Figure 2-2A). A midpoint potential of approximately 0 mV versus the standard hydrogen electrode (SHE) was observed at pH 7.0 ($E_{M,7}$) for the wild-type protein. The pH dependence of the mNT potential is modeled well assuming a one-electron process that is coupled to one distinct protonation event.

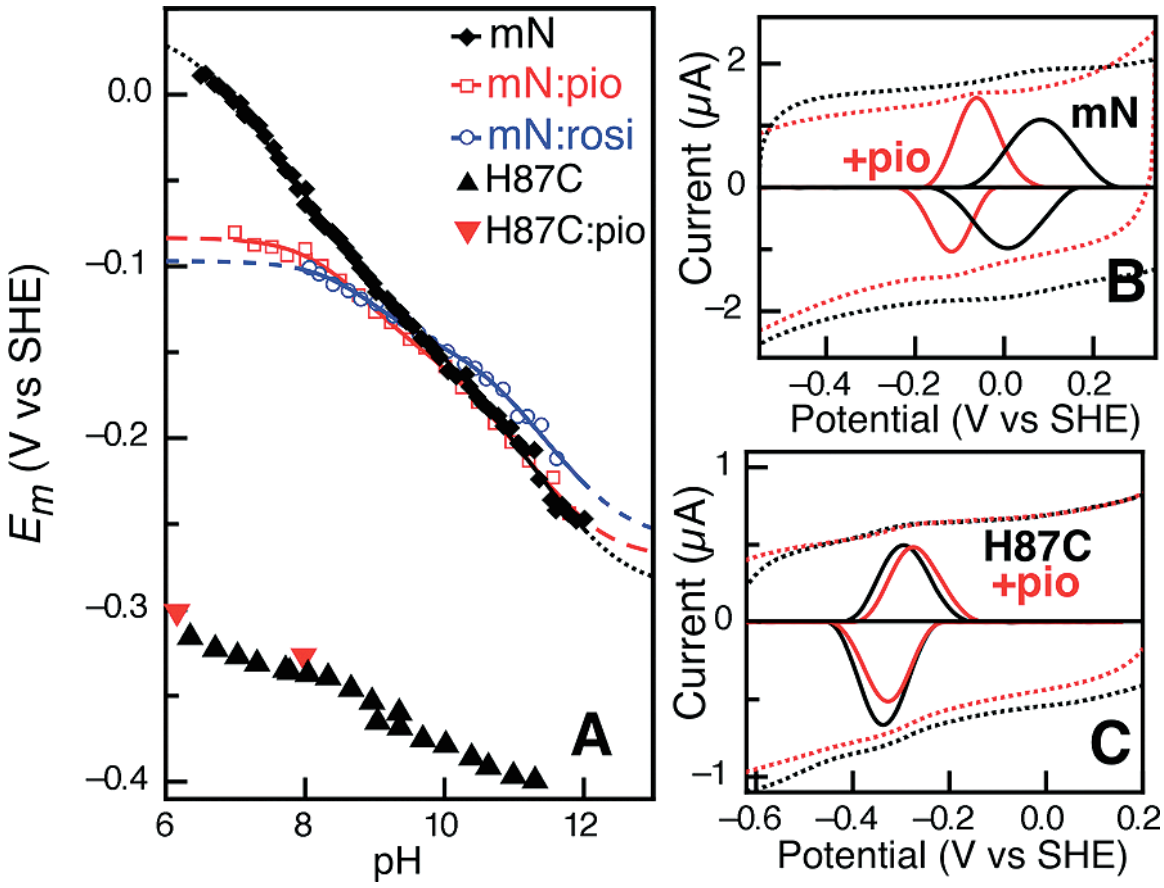

Figure 2-2: mNT's redox properties are modulated by TZD binding. (A) Comparison of wild-type mNT (mN) pH dependence of midpoint potentials in the TZD-free (black diamonds) and pioglitazone- and rosiglitazone-bound states (red squares and blue circles, respectively). Voltammogram of the H87C mutant (black triangles) and H87C treated with pioglitazone (red triangles). (B) Raw and baseline-subtracted data for mN alone (black dotted and solid lines, respectively) and in the presence of pioglitazone (red). (C) Analogous data for the H87C mutant in the absence and presence of the TZD drug (28).

DISCUSSION

Using PFV analyses, we have interrogated the connection between redox chemistry of mNT and TZD drug binding. Data from both the pioglitazone-bound (Figure 2-2B) and rosiglitazone-bound forms of mNT yield pH-dependent ($E_{M,7}$) values shown in Figure 2-2A (red and blue). Both TZD bound forms of mNT display similar changes: in both cases, the reduction potential is lowered at pH values near neutral, and the decrease in potential can be ascribed to an increase in pK_{ox} that occurs upon drug binding. The shift in pK_{ox} results in a decrease in ($E_{M,7}$) of ~100 mV for the TZD-bound forms of mNT, where other perturbations to the pH dependence curve upon drug binding are minor.

Presently available crystallographic analyses yield promising possibilities for the identities of site(s) of protonation and drug binding. In analogy to Rieske FeS proteins (34), it is most likely that the site of redox-linked protonation is ε−N of the cluster ligand His87. However, the mNT [2Fe-2S] cluster environment does display other differences with respect to Rieske proteins, including a lysine residue positioned within ~4 Å of His87 ε-N. A conserved bridging water molecule could theoretically create a hydrogen bond network between His87 and Lys55 (Figure 2-3), providing an alternative arrangement that leads to proton coupling at His87.

While articulating the details of the mechanism of proton coupling will remain a future challenge, it is clear that His87 is critically important. Replacement of His87 with Cys results in a dramatic decrease in the midpoint potential by more than 300mV (Figure 2-2C) to a value of - 320 mV at pH 7, suggestive of [2Fe-2S] 4-Cys ferredoxins (16).

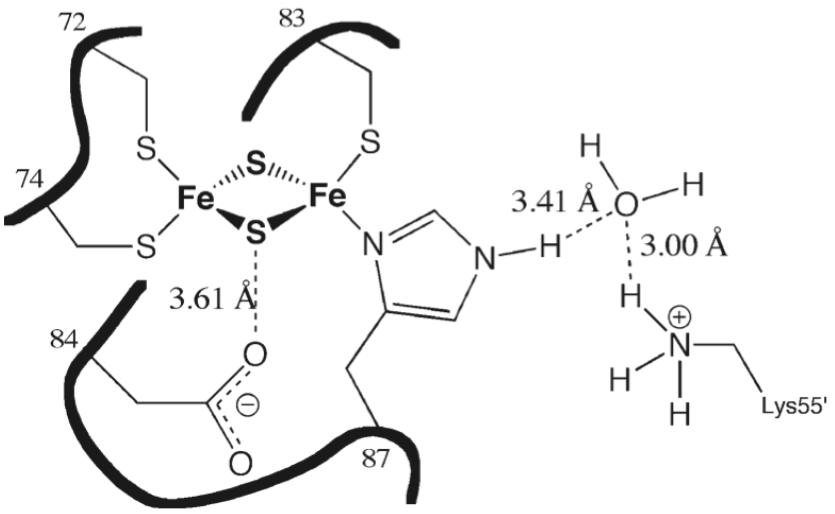

Figure 2-3: Schematic of the [2Fe-2S] cluster of mNT surrounded by ligating residues. Cys72, Cys74, Cys83, and His87 and important ionizable residues Asp84 and Lys55. Potential hydrogen bonds are represented by dashed lines and distances by dotted lines. All distances are averages between non-hydrogen atoms from mNT PDB entries 2QH7, 2R13, and 2QD0 (28).

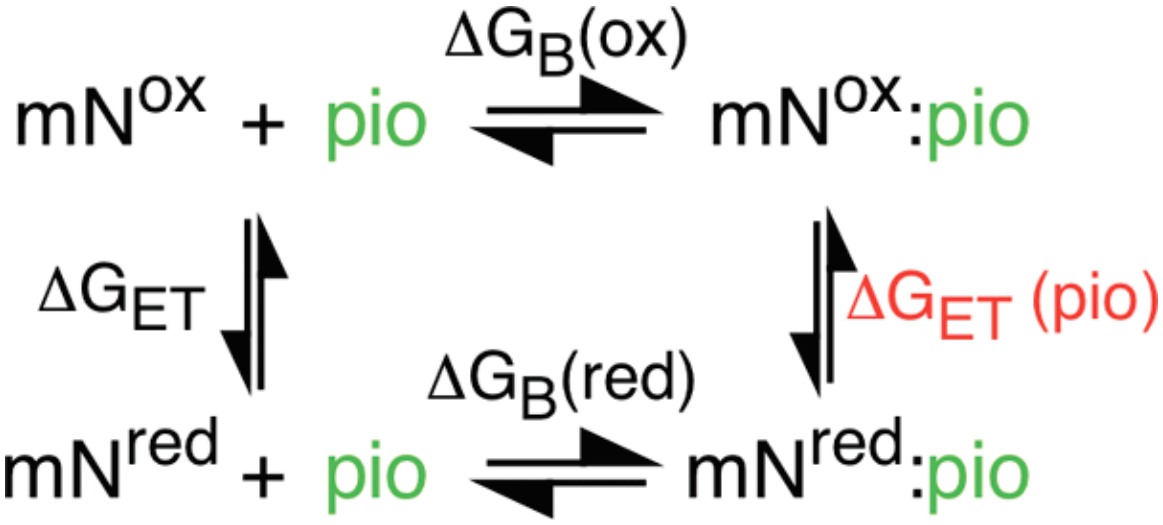

Figure 2-4: TZDs bind preferentially to oxidized mNT. Thermodynamic square relating free energies of binding of pioglitazone to mNT in the oxidized and reduced states. $\Delta G_{ET} = -nFE_{M,7}$, where n is the number of electrons, F is Faraday's constant, and ($E_{M,7}$) is the redox potential (28).

The overall pH-dependence becomes much more nondescript with an apparent linear slope of -15 mV/pH unit. Most importantly, upon treatment of the H87C mutant with pioglitazone, a nominal change in potential is observed, a positive shift of 5 mV. Taken together, the H87C mutant data suggest that a significant component of the interaction of the TZD drug with mNT occurs via His87, resulting in the modulation of the redox-linked pK_{ox} and, therefore, the midpoint potential. Notably, this interaction may be through direct hydrogen bonding or van der Waals interactions or might be through an allosteric mechanism of drug binding to another site on mNT.

A clear challenge in this field is to understand TZD drug binding at a higher level of detail. Measuring association constants for TZD binding has not yet been accomplished because of the high insolubility of the drugs in aqueous buffers, and solubility of the drug requires high concentrations of DMSO, which denature mNT upon prolonged exposure, as required in equilibrium titrations. Here PFV has the benefit of probing relatively low concentrations of mNT at an electrode (subpicomolar), such that the insolubility of the drug is not an issue. From the overall shift of the Em values, one can determine the ratio of relative affinities for the drug to the oxidized and reduced states of the protein based on the thermodynamic square shown in Figure 2-4. Using the Nernst equation, we can find a ratio for the ΔG values for pioglitazone binding to the oxidized and reduced states as illustrated in Figure 4-4 and, thereby, the ratio of affinities (directly related to the free energies of binding). This estimate shows that the drug binds the oxidized state with a roughly 50-fold higher affinity than it does the reduced state.

Collectively, our data may explain the role of the drug in alleviating oxidative stress. MNT is most likely to be found in its reduced state under physiological conditions;

on the basis of the reducing environment of the cytosol (35) and the potential of ~0 mV at pH 7, the overall lowering of ($E_{M,7}$) due to drug binding will make mNT a better reducing agent, which may be beneficial under oxidative stress conditions. At the same time, the enhanced TZD affinity for the oxidized form of mNT reflects thermodynamic stabilization of the oxidized [2Fe-2S] cluster, when the drug is bound. It has been appreciated that at pH <7 the [2Fe-2S] cluster of mNT is labile, and that pioglitazone binding counteracts lability, as does a H87C mutation (12). Under oxidative stress conditions, cluster oxidation and subsequent lability may be a significant issue that TZD binding counteracts.

CONCLUSION

Here we have observed for the first time that two members of the TZD drug family similarly affect mNT redox chemistry: pK_{ox} increases by ~2 units, and this results in an ($E_{M,7}$) reduced by ~100 mV. Thus, drug binding has a fundamental impact on the redox activity of mNT. Previous spectroscopic evidence has demonstrated that mNT can exist in both reduced and oxidized forms (11), and that TZD drug binding impacts the redox properties of the [2Fe-2S] cluster of mNT, likely via His87. We show that PFV can serve as a tool in further assessing the impact of TZD drug binding in this emerging class of FeS proteins related to oxidative stress, mitochondrial function, and type 2 diabetes.

Chapter 2, in part, is a reprint of the material as it appears in Biochemistry by Bak DW, Zuris JA, Paddock ML, Jennings PA, Elliott SJ. 48 2009. The dissertation/thesis author was a contributing investigator and contributing author in this paper.

Chapter 3

Engineering the Redox Potential over a Wide Range within a New Class of FeS Proteins

ABSTRACT

MitoNEET (mNT) is a newly discovered mitochondrial protein and a target of the TZD class of anti-diabetes drugs. MNT is homodimeric with each protomer binding a [2Fe-2S] center through a rare 3-Cys and 1-His coordination geometry. Both the fold and the coordination of the [2Fe-2S] centers suggest that it could have novel properties compared to other known [2Fe-2S] proteins. We tested the robustness of mNT to mutation and the range over which the redox potential (E_M) could be tuned. We found that the protein could tolerate an array of mutations that modified the E_M of the [2Fe-2S] center over a range of ~700 mV, which is the largest E_M range engineered in an FeS protein and, importantly, spans the cellular redox range (+200 to -300 mV). These properties make mNT potentially useful for both physiological studies and industrial applications as a stable, water soluble, redox agent.

INTRODUCTION

Iron sulfur (FeS) proteins are integral players in a vast array of biological activities from redox chemistry in respiration and photosynthesis to the regulation of transcription and gene expression (19). They perform these many diverse functions using only a small set of different FeS moieties, and their functions are largely derived from the protein environment around the FeS centers (19). In particular, tuning the redox potential (E_M) of the FeS center is critical for controlling the conditions under which the protein responds to its environment and its interacting partners. As a class, FeS proteins span a wide redox range (19) under normal cellular conditions, indicating that FeS centers are fundamentally tunable. This broad redox range is achieved using several different protein scaffolds.

Progress has recently been made in tuning the E_M over a large range within the same protein scaffold of two non-FeS proteins, a cupredoxin (36) and a superoxide dismutase (37). The upper E_M limit of both of these systems is close to +1 V, which indicates that these proteins could be useful catalysts in key chemical redox processes such as water oxidation (20, 37) However, neither system could access the solution potentials in cellular environments (-300 mV to +200 mV) (38). Because different FeS proteins naturally span this range (19), we rationalized that the E_M of a single FeS protein could be engineered to span both above and below the cellular solution range. Such a class of proteins could serve as reporters of cellular redox or be used to perturb the normal E_M of the cellular solution. Here, we report our success in tuning the E_M of the [2Fe-2S] center of the outer mitochondrial membrane protein mNT over a range of 700 mV, which is the largest E_M range engineered in an FeS protein and, importantly, spans the cellular redox range.

EXPERIMENTAL METHODS

Protein Expression and Purification: Over-expression and purification of mNT proteins were performed as outlined (39).

Optical Spectroscopy and pH Titrations: All UV-Visible absorption spectra were measured from the near UV to the near IR (300 - 700 nm) on a Cary50 spectrometer (Varian Inc, Palo Alto CA) equipped with a temperature-controlled cell (T = 25°C) (50-100 μM protein in 25 mM Tris-HCl, 100 mM NaCl, pH 8 buffer). The pK_{ox} of His87 when the [2Fe-2S] centers are in the oxidized state was determined by monitoring the shift in the wavelength peak position as a function of pH:

$$\lambda_{obs} = \lambda_{unprot} + \Delta\lambda / (1 + 10\text{^}(pH - pK_{ox})) \qquad \text{(Equation 1-1)}$$

where λ_{obs} is the observed maximum peak value near 458 nm at a given pH for the species under investigation, λ_{unprot} is the wavelength peak when His87 is deprotonated, and $\Delta\lambda$ is the difference between the wavelength of the fully protonated species and the fully unprotonated species. The pK_{red} of His87 when the [2Fe-2S] centers are in the reduced state was determined similarly using the equation below:

$$\lambda_{obs} = \lambda_{unprot,\ red} + \Delta\lambda / (1 + 10\text{^}(pH - pK_{red})) \qquad \text{(Equation 1-2)}$$

where $\lambda_{unprot,\ red}$ is 546 nm (for WT) or 544 nm (for K55E) and represents the reduced peak that undergoes a shift at high pH. As in Eq. S1, λ_{obs} , $\Delta\lambda$, and pH are the observed wavelength, the difference in peak wavelength (546 nm vs. 553 nm) between the pH extremes, and the [H+], respectively.

Optical Redox Titrations: A detailed explanation of optical titration methods can be found in Dutton et al (40). The reduction state was determined by monitoring the absorbance at 458 nm with 100 μM mNT for both WT and mutants under appropriate buffer conditions, depending on pH. The ambient redox potential was adjusted by adding dithionite and measured with a Ag/AgCl dual reference and working electrode (Microelectrodes Inc, Bedford NH), and potentials were adjusted to Standard Hydrogen Electrode (SHE) values for presentation. The accuracy of the Ag/AgCl electrode was checked after each experiment using a set of quinone/quinhydrone standards (Sigma-Aldrich) as recommended by the manufacturer. An elixir of redox mediators was used to ensure equilibration and stability. All mediators were purchased from Sigma-Aldrich and were chosen to span the potential region of both the WT protein and the mutants in this study. The mediators employed and their respective concentrations were: 1,4-benzoquinone (50 μM), methylene blue (25 μM), menadione (50 μM), 1,4-

naphthoquinone (25 μM), anthraquinone-2-sulfonate (25 μM), dithiothreitol (50 μM), and methyl viologen (2 μM). Absorbance values at 458 nm were converted to fraction oxidized, in which the fully oxidized 458 nm peak corresponded to 1.0 and the fully reduced 458 nm peak corresponded to 0.0. The equation is given below:

$$\text{Fraction Oxidized} = (A_{obs} - A_{red}) / (A_{ox} - A_{red}) \qquad \text{(Equation 1-3)}$$

where A_{obs} is the measured absorbance at a given potential, A_{red} is the absorbance of the fully reduced sample, and A_{ox} is the absorbance of the fully oxidized sample. Origin 6.1 (OriginLab Corporation) was used to determine the E_M from a fit of the fraction oxidized versus potential using the Nernst equation below:

$$\text{Fraction Oxidized} = 1/(1 + 10[(E_M - E^0)*n/59.1\ \text{mV})]) \qquad \text{(Equation 1-4)}$$

where E_M is the redox midpoint potential of the species, E^0 is the ambient cell potential corresponding to each fraction oxidized, and n is the number of electrons in the chemical reaction. Optical redox titration data was fit to a pKa using the equation below:

$$E_M = E_{acid} + 2.303(RT/nF)*\log(([H+] + K_{a\ red})/([H+] + K_{a\ ox})) + \alpha(pH) \qquad \text{(Equation 1-5)}$$

where E_M is the measured redox potential of the species under study, E_{acid} is the redox potential limit at low pH, R is the universal gas constant, T is temperature measured in K, n is the number of electrons involved in the chemical reaction, F is Faraday's constant, [H+] is the concentration of protons in solution, and $K_{a\ ox}$ and $K_{a\ red}$ are the proton equilibrium constants for the oxidative reaction and reductive reaction, respectively. We also introduce α(pH) as a global factor to account for all pH-dependent changes from pH 6 to 11 other than titration of His87, which is explicitly treated. To first order we have treated α(pH) as α*pH. It introduces an overall decrease in magnitude of the slope that amounts to ~15%. For the H87C mutant, there is no His87 titration and so the equation

reduces to $E_M = E_{acid} + \alpha(pH)$, with α accounting for the shallow pH dependence that is observed in Figure 3-3B. Units for the E_M are reported in millivolts (mV).

Protein-film voltammetry: A detailed description of protein-film voltammetry can be attained from previous work (34). Protein-film voltammograms were generated using a CHI 730C Electrochemical Workstation (CH Instruments Inc., Austin TX) equipped with an in-house glass electrochemical cell supporting a working electrode, a 3 M Ag/AgCl reference electrode, and platinum wire counter electrode. The working electrode was purchased from ALS (Tokyo, JP) and was comprised of highly oriented edge-plane graphite (HOPG) with a surface area of 7 mm^2. Preparation of protein films and the choice of buffers for different pH measurements were performed as reported previously (28). The glass cell and the sample buffer were chilled in a 4 °C water bath. Scan rates were performed at 200 mV/s over a range from +0.5 V to -0.6 V vs. SHE. No changes in E_M outside of the normal uncertainty (±5 mV) in measurements were observed over scan rates from 50 mV/s to 400 mV/s. No appreciable shifts (± 5 mV) in E_M were observed in the WT by going to either higher salt concentrations (1 M) or switching to different buffers. All measurements were taken at 4 °C to enhance the amplitude of the anodic and cathodic peak potentials (28), and spot checking measurements at 25 °C showed the same results within uncertainty (±5 mV). Baseline subtraction of voltammetry data was performed using the SOAS software package, courtesy of Christopher Leger (41). All data were obtained using the Ag/AgCl reference electrode (+205 mV SHE) and checked for accuracy using methylene blue (Sigma-Aldrich) as a standard. Measurements were corrected to SHE for presentation. A systematic shift of -25 ±4 mV was observed for PFV compared to the optical method. The E_M for D84G at pH

6.0 was measured using PFV and was shifted by + 25 mV for comparison with the optical redox titration E_M values shown in Figure 3-3.

RESULTS AND DISCUSSION

MNT is a newly discovered mitochondrial target of the TZD class of anti-diabetes drugs, such as pioglitazone (Actos) and rosiglitazone (Avandia) (9). Human mNT defines a unique class of [2Fe-2S] proteins. The crystal structure shows that mNT is a homodimer, with each protomer binding a [2Fe-2S] center through a rare 3-Cys and 1-His coordination geometry (Figure 3-1) (12-14). Both the fold and the coordination of the [2Fe-2S] centers suggest that mNT could have novel properties compared to other known [2Fe-2S] proteins. For example, the unusual coordination of the [2Fe-2S] center contributes to the atypical proton-coupled ($E_{M,7}$) of +25 mV at pH 7.0 (39). We used optical potentiometric redox titrations (40) and protein-film voltammetry (42) to assess changes in the $E_{M,7}$ resulting from mutagenesis of first and second shell residues near the [2Fe-2S] center. Single and double mutations were designed to test both the robustness of the [2Fe-2S] center and the E_M range that could be achieved. We found that the E_M could be tuned over a wide range (Figure 3-2, Table 1). As a first step, we needed to improve our characterization of the WT. We had previously shown that the E_M of WT mNT is pH-dependent above neutral pH, indicating that reduction is coupled to proton uptake (28, 39). Optical potentiometric redox titrations indicated that the [2Fe-2S] cluster of mNT undergoes a one-electron reduction step: $[2Fe\text{-}2S]^{2+}/[2Fe\text{-}2S]^{+}$:H (Figure 3-3). At a pH just above its pK_{ox}, uptake of a proton occurs upon reduction, resulting in a pH-dependence for the E_M (28). This occurs up to the point where the pH matches the pK_a of the proton in the reduced state (pK_{red}). The most likely candidate for a site of protonation

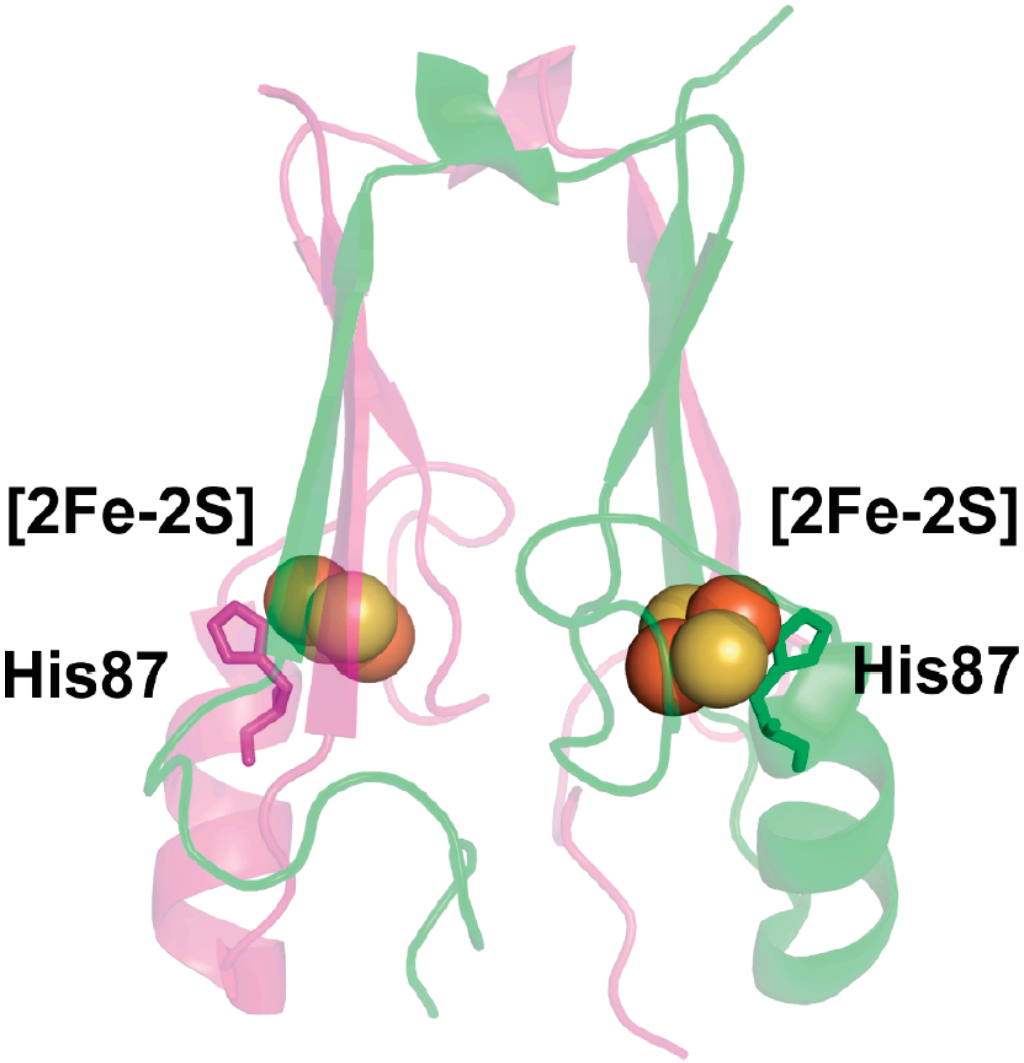

Figure 3-1: Protein backbone of the cytoplasmic exposed domain of the outer-mitochondrial membrane protein mNT (PDB code 2QH7) showing the redox active [2Fe-2S] centers. mNT is a homodimer (12) with one protomer shown in magenta and the other in green. Each protomer contains a [2Fe-2S] center (shown as spheres) coordinated by 3-Cys and 1-His, with the hallmark single-coordinating His87 indicated. The distance between the [2Fe-2S] centers is ~16 Å from center-to-center. His87 coordinates to the outer, more solvent exposed, Fe of the [2Fe-2S] center, where the electron is predominantly localized upon reduction (43).

in the WT mNT is His87 (Figure 3-4A), which shows pH-dependent vibrational interactions with the [2Fe-2S] center (44, 45). His87 is ligated to the outermost Fe of the [2Fe-2S] center, where, upon reduction, the additional electron is predominantly localized (44). In addition, pulsed EPR studies indicated that His87 is protonated in the reduced state (44). At the appropriate pH, protonation of His upon reduction is observed in redox studies on Rieske type [2Fe-2S] centers that involve His coordination (34). His87 will contribute to the observed proton-coupled reduction in the pH range above its pK_{ox} and below its pK_{red}. In a previous study, detailed PFV data were fit to two models (28). Both models included His87 as an integral player in proton coupling to electron reduction but differed in the pH range over which protonation of His87 contributed to the pH dependence. Here, we use direct UV-vis titration (46) as an independent method to determine the pH range over which His87 contributes to the proton coupling. This allows us to distinguish between the two models. We measured the UV-vis region as a function of pH, as differences in the absorption peaks are expected to reflect the state of protonation of the titrating ligand (46). Indeed, changes in the absorbance peak position of the WT protein in the oxidized state were sensitive to pH and indicated a titration with an apparent $pK_{ox} = 6.8 \pm 0.2$ (Figure 3-5A). In addition, peak changes in the reduced state indicated that the pK_{red} was 12.4 ± 0.2 (Figure 3-5B). This value is consistent with values for pK_{red} of ~12.5 reported for the coordinating histidine ligands found in Rieske centers (34). The lack of spectral changes in the H87C mutant

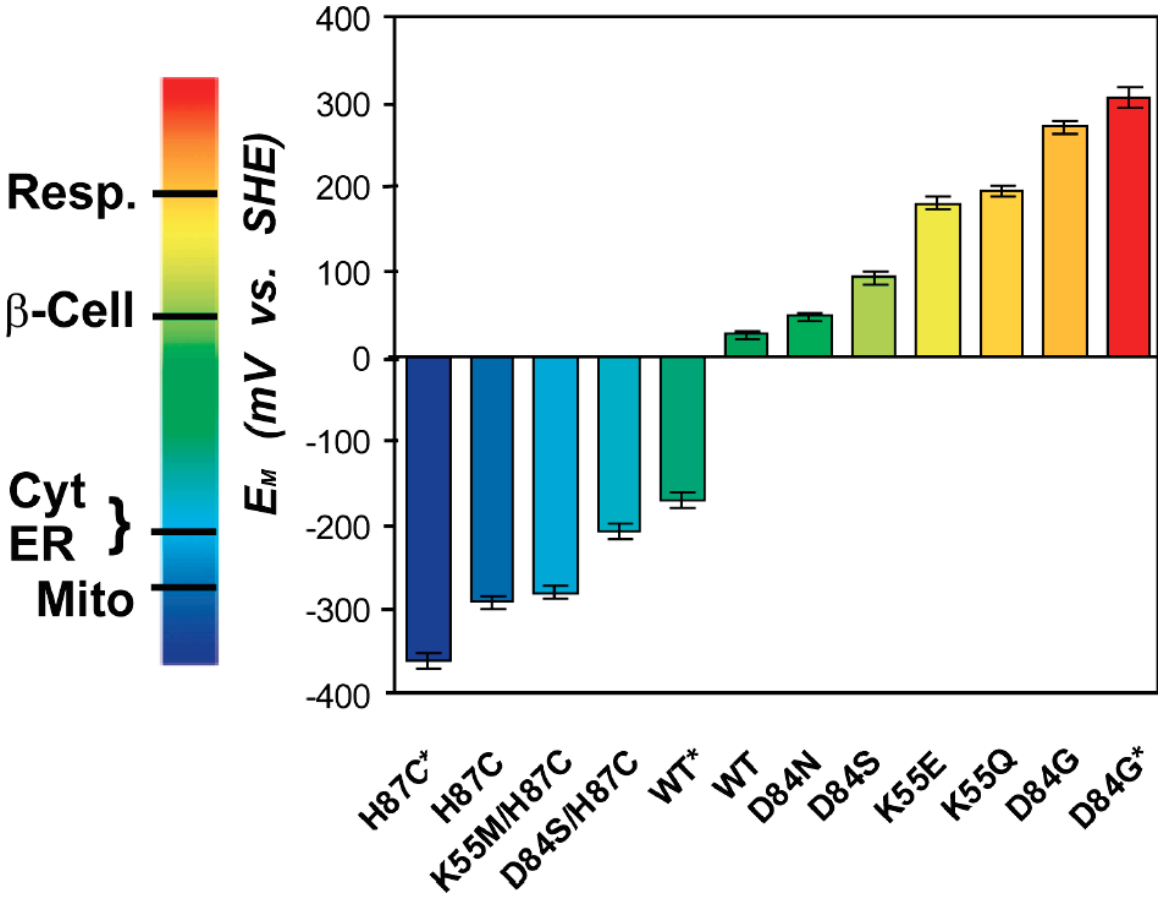

Figure 3-2: E_M values of WT and mutant mNT have been engineered over a range of ~700 mV and can be tuned to obtain nearly any value within the E_M range shown (43). Measurements adjusted to SHE values, with errors (10 mV) indicated by cross bars. *E_M extremes (see Figure 3-4B). The E_M values of several cellular environments are shown on the left bar. Abbreviations: Resp. (Respiratory tract fluid, +200 mV), β-Cell (Cytoplasm of beta cells, producers of insulin in the pancreas, +55 mV), Cyt (Cytoplasm, -205 mV), ER (Endoplasmic Reticulum, -217 mV), Mito (Mitochondria, -260 mV) (38).

Table 3-1: Redox Potentials of mNT and mutants

mNT Mutant	$E_{M,7}^{Opt}$ (mV)	$E_{M,7}^{PFV}$ (mV)
WT	+25	0
K55E	+185	+166
K55Q	+200	+176
S77A	-2	n.a.
D84E	+66	n.a.
D84G	+270	+255
D84N	+48	+19
D84S	+90	n.a.
H87C	-290	-320
K55M/H87C	-270	n.a.
D84S/H87C	-210	n.a.

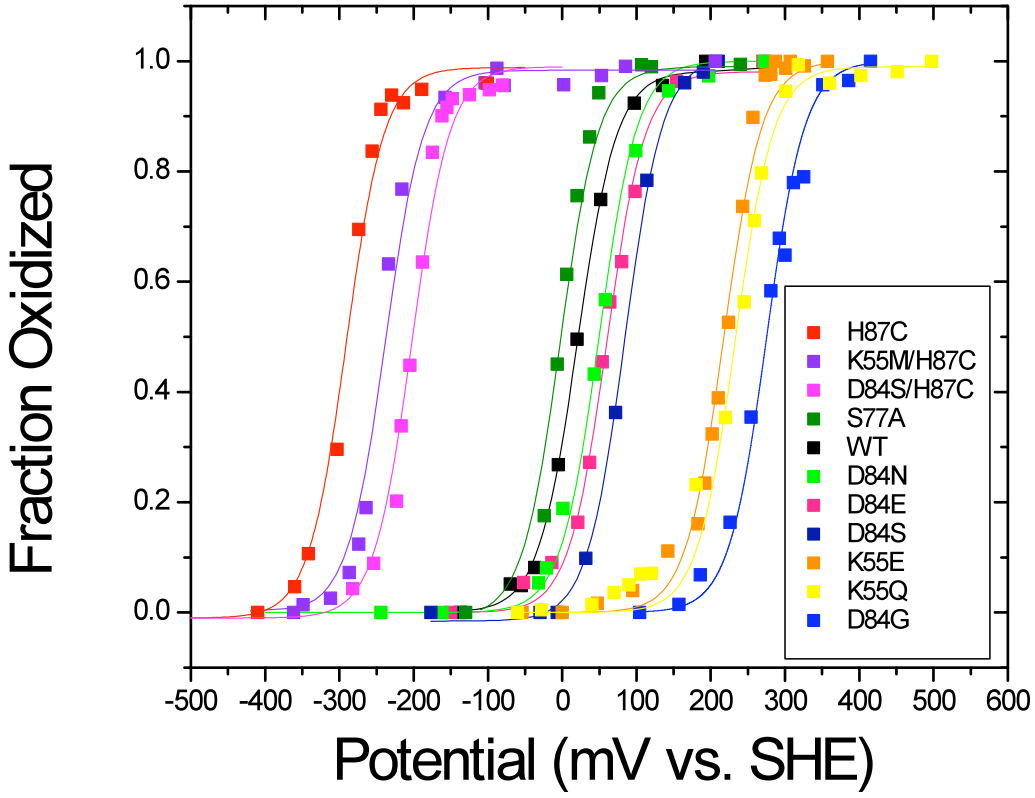

Figure 3-3: Measurements and fits of optical titration data of WT mNT and several mutants at pH 7.0. All samples were measured in 100 mM Bis-Tris pH 7.0. Data were fit to a Nernstian curve (Equation 1-4). $E_{M,7}$ values of each mNT mutant, in order from left to right, are as follows: H87C (-290 mV), K55M/H87C (-270 mV), D84S/H87C (-210 mV), S77A (-2 mV), WT (+25 mV), D84N (+48 mV), D84E (+66 mV), D84S (+90 mV), K55E (+185 mV), K55Q (+200 mV), D84G (+270 mV) (43).

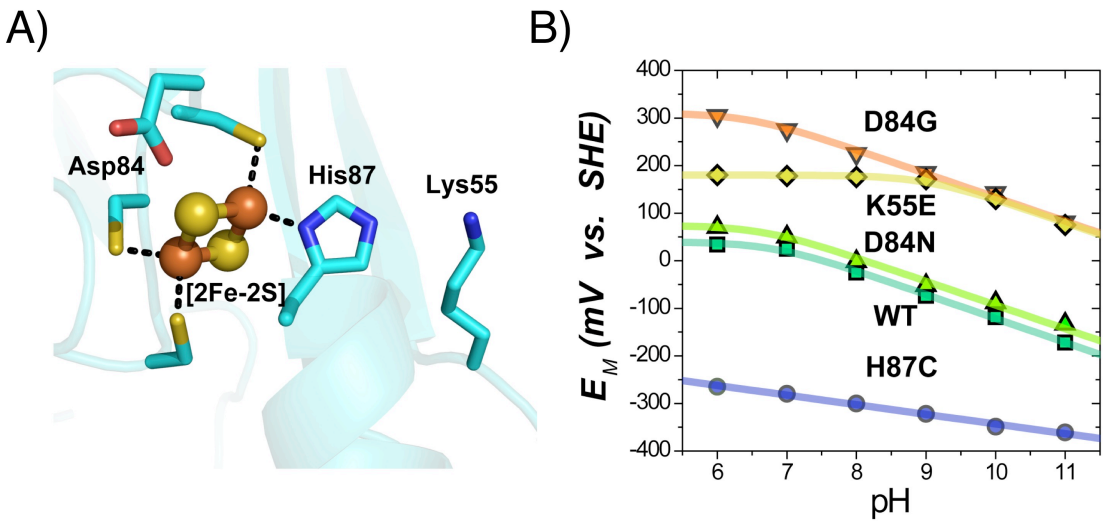

Figure 3-4: Effects of different local residues on mNT's redox properties. (A) Structure near the [2Fe-2S] center (Fe atoms as red spheres, sulfur as yellow) of mNT showing both the ligating and nearby (<5 Å) titratable residues. (B) Representative pH dependences of the EM for select mutants. WT, D84G, and D84N exhibit similar dependences (-51 mV/pH) at pH >6.8, implying that, in these cases, reduction remains proton coupled. H87C shows a more-shallow slope (-15 mV/pH) for the pH-dependence, 10 indicating that His87 is principally responsible for the observed proton coupling in WT. Replacement of Lys55 with Glu (K55E) shifts the pK_{ox} of His87 from 6.7 ± 0.2 to 9.2 ± 0.2 (43).

confirms the assignment of these changes to the protonation of His87. Thus, protonation of His87 is predominantly responsible for the pH-dependence of the E_M over the entire range of pH measured in this study. These new data required a refinement of the previous model used to describe the pH-dependence data (28). In the refined model, we explicitly include His87 as a major contributor to the observed titration across the entire measured range and implicitly include other groups and pH-dependent effects in a factor α (Equation 1-5). Fitting of the data to the model (Figure 3-5B) yields values of pK_{ox} = 6.7 ± 0.2 and pK_{red} > 11.5 for His87, which is in agreement with the values determined from UV-vis pH titration, giving us confidence that the refined model provides an adequate explanation of the measured data.

We continued our mutant survey by replacing the single coordinating His ligand (His87) with Cys (Figure 3-4A). Initial studies showed that replacement of His87 with Cys (H87C) results in a significantly more stable protein with an $E_{M,7}$ shifted from +25 mV to -290 mV, decreasing to -360 mV at pH 11.0 (Figure 3-4B). The recently determined crystal structure17 (PDB ID code 3LPQ) showed that the Sγ of Cys87 in the H87C mutant replaced the Nδ of His87 in the WT as a ligand of the outer Fe of the [2Fe-2S] center, with no observed long-range structural changes. The shift to a more negative $E_{M,7}$ can thus be attributed to the substitution of the neutral His with an anionic Cys ligand (47) at the 87 site. This finding was consistent with previous reports (28) and demonstrates that His87 is a critical ligand in tuning the E_M.

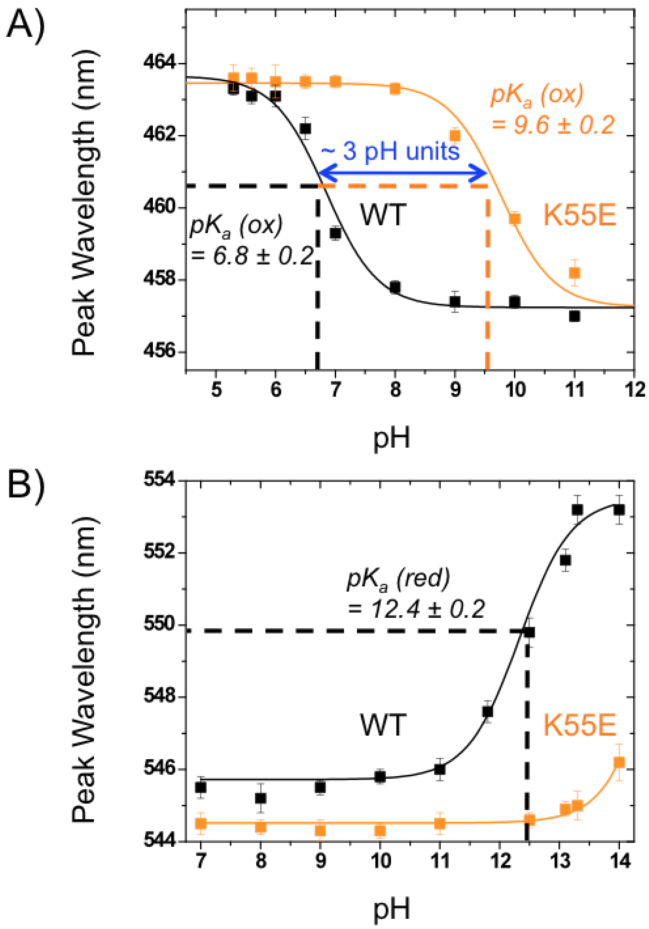

Figure 3-5: Optical pH indicate that His87 is source of pH dependent E_M. A) Optical pH titration shifts for WT mNT (black squares) and the K55E mutant (orange squares) in the oxidized state. Data were fitted to a pH titration equation (Equation S1) and showed a single titration from pH 5 to 14. Spectra indicate that the pK_{ox} of N-ε on His87 shifts from 6.8 ± 0.2 in the WT to 9.6 ± 0.2 in the K55E mutant. Peak wavelength values at 463 nm correspond to protonated His87, whereas those at 457 nm correspond to deprotonated His87. B) Optical pH titration shifts for WT and the K55E mutant in the reduced state fit with Equation 1-2. The pK_{red} for His87 in the WT in was determined to be 12.4 ± 0.2. The H87C mutant showed no shifts in either state, confirming the assignment of the single titrating group to His87 (43).

Having established that His87 is a critical ligand in tuning the E_M, we next targeted Lys55, which is located ~4 Å from His87 (Figure 3-4A). Based on its close proximity to His87, along with the observed changes in the side chain conformation of Lys55 in the H87C mutant (47) we anticipated that replacing the cationic Lys55 with neutral or negative side chains would increase the pK_{ox} of His87 and thereby the $E_{M,7}$ of the mutant protein (48). Replacement of Lys55 with the neutral Gln (K55Q) or anionic Glu (K55E) both resulted in $E_{M,7}$ values of ~ +200 mV (Figure 3-2, Table 3-1). The similar $E_{M,7}$ values for the K55E and K55Q mutants indicate that their predominant effect on $E_{M,7}$ is caused by removal of the cationic Lys. A fit of the data to the model (Equation 1-5) yielded a pK_{ox} of His87 in the K55E that was shifted by ~3 pK_a units to 9.2 ± 0.2 (Figure 3-4B). This was confirmed by optical pH titrations, which gave a value of 9.6 ± 0.2 (Figure 3-5A). In the WT, Lys55 makes an inter-protomer interaction with the hydrogen on N-ε of His87. Removal of this H-bond should affect the interprotomer contact, which would have additional consequences on the stability of the reduced [2Fe-2S] centers, consistent with the unexpectedly higher E_M observed even at lower pH (Figure 3-3B). We have shown that replacement of a charged group next to a coordinating His can dramatically affect both the pK_{ox} of the His and the E_M of the [2Fe-2S] center. Another titratable side chain located near the [2Fe-2S] center is Asp84 (Figure 3-3A). Asp84 is within hydrogen bonding distance to the proximal inorganic sulfur of the [2Fe-2S] center, suggesting that Asp84 may be in the protonated state. This was confirmed by replacement with Asn (D84N), which resulted in E_M values similar to the case of the WT over a pH range from 6.0 to 11.0 (Figure 3-4B). Similar values were

obtained upon replacement with Glu (D84E) and Ser (D84S) (Figure 3-2, Table 3-1). The D84S/H87C double mutant showed that the effects of the two mutations on the $E_{M,7}$ were additive (Figure 3-2, Table 3-1), which suggests that further unique $E_{M,7}$ values could be obtained with double mutants utilizing sites 84 and 87.

Surprisingly, replacement of Asp84 with Gly (D84G) resulted in a much more positive $E_{M,7}$ of +270 mV (Figure 3-2), increasing to +305 mV at pH 6.0 (Figure 3-4B). This is not a result of gross structural changes, as the optical spectrum of the D84G mutant is similar to that for the WT (Figure 3-6). However, the D84G mutation likely alters the solvent accessibility of the cluster, which has been shown to strongly affect $E_{M,7}$ values in other FeS systems, such as Rieske centers (49).

CONCLUSION

We have shown that mNT is amenable to manipulation of residues located near the [2Fe-2S] centers. We were able to tune the E_M over a range of ~700 mV. This system's resultant range of $E_{M,7}$ values is beyond that of any previously reported FeS protein. Combined with pH modulation, the E_M of the [2Fe-2S] center can be tuned to essentially any value within a range from -360 mV to +305 mV, making it potentially useful for both physiological studies as well as in industrial applications as a stable, water-soluble, redox agent.

Chapter 3, in part, is a reprint of the material as it appears in Journal of the American Chemical Society by Zuris JA, Halim DA, Conlan AR, Abresch EC, Nechushtai R, Paddock ML, Jennings PA. 132 2010. The dissertation/thesis author was the primary investigator and author of this paper.

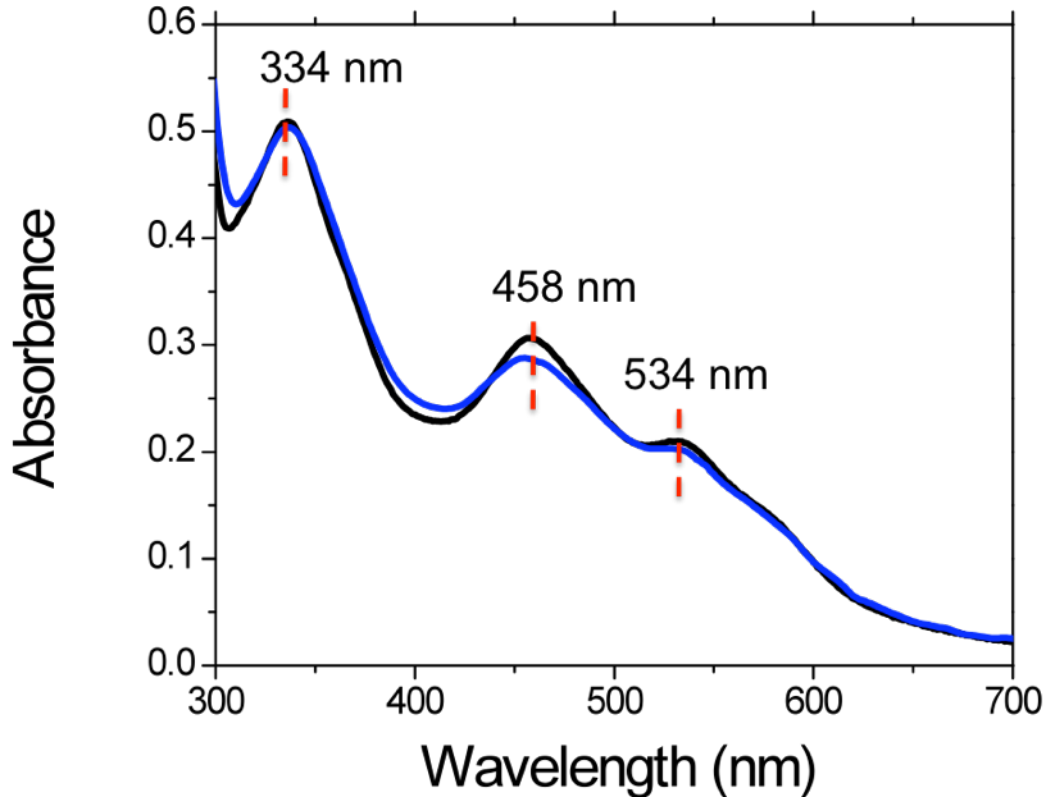

Figure 3-6: Optical Spectra of WT mNT (black) and the D84G (blue) mutant. Samples were measured in 50 mM Tris 100 mM NaCl. Optical spectra indicate similar coordination geometries for the WT and D84G as the signature peak at 458 nm appear to be similar in both species. Peaks at 334 nm and 534 nm are also very similar. In contrast, the H87C mutant displays large changes (47) at the 458 nm peak, with a significant shoulder appearing near 420 nm as previously reported (43).

Chapter 4

Facile Transfer of [2Fe-2S] Clusters from the Diabetes Drug Target MitoNEET to an Apo-acceptor Protein

ABSTRACT

MitoNEET (mNT) is an outer mitochondrial membrane target of the thiazolidinedione class of diabetes drugs with a unique fold and a labile [2Fe-2S] cluster. The rare 1-His and 3-Cys coordination of mNT's [2Fe-2S] leads to cluster lability that is strongly dependent on the presence of the single histidine ligand (His87). These properties of mNT are similar to known [2Fe-2S] shuttle proteins. Here we investigated whether mNT is capable of cluster transfer to acceptor protein(s). Facile [2Fe-2S] cluster transfer is observed between oxidized mNT and apo-ferredoxin (a-Fd) using UV-vis spectroscopy and native-PAGE, as well as with a mitochondrial iron detection assay in cells. The transfer is unidirectional, proceeds to completion, and occurs with a second-order-reaction rate that is comparable to known iron-sulfur transfer proteins. Mutagenesis of His87 with Cys (H87C) inhibits transfer of the [2Fe-2S] clusters to a-Fd. This inhibition is beyond that expected from increased cluster kinetic stability, as the equivalently stable Lys55 to Glu (K55E) mutation did not inhibit transfer. The H87C mutant also failed to transfer its iron to mitochondria in HEK293 cells. The diabetes drug pioglitazone inhibits iron transfer from WT mNT to mitochondria, indicating that pioglitazone affects a specific property, [2Fe-2S] cluster transfer, in the cellular environment. This finding is interesting in light of the role of iron overload in diabetes. Our findings suggest a likely role for mNT in [2Fe-2S] and/or iron transfer to acceptor proteins and support the idea that pioglitazone's anti-diabetic mode of action may, in part, be to inhibit transfer of mNT's [2Fe-2S] cluster.

INTRODUCTION

MitoNEET (mNT) is a newly discovered target (9) of the insulin- sensitizing thiazolidinedione (TZD) class of type 2 diabetes drugs (50, 51), which interact with the canonical target PPARγ (52, 53). The interaction of TZD drugs with mNT has been proposed to be of therapeutic importance (9, 12). The protein contains two [2Fe-2S] clusters, which have been shown to be chemically labile (11). Initial characterization of mNT's redox active and pH labile [2Fe-2S] clusters show that both properties are modulated by TZDs (12, 28). A second related member of the human NEET protein family, Miner1, is structurally homologous to mNT (39). Miner1 has recently been linked to autophagy, apoptosis, and aging (26, 27, 54), and mis-splicing is associated with a rare disease, known as Wolfram Syndrome 2 (23). Together, mNT and Miner1 represent a new class of NEET iron-sulfur (FeS) proteins characterized structurally by their unique homodimeric fold and rare 3-Cys-1-His [2Fe-2S] cluster ligand environment (12-14).

Iron-sulfur (FeS) cluster-containing proteins are key players in many essential processes, such as photosynthesis, respiration, and nitrogen fixation (17, 55). They appear in various compositions and confer upon FeS proteins the ability to accept or donate single electrons and/or iron, catalyze enzymatic reactions, or even function as regulatory proteins (21). Disruption of FeS cluster biogenesis is deleterious to vital cell processes in humans, leading to diseases such as Friedreich's ataxia (56), X-linked sideroblastic anemia with ataxia (XLSA/A) (57), and a form of sideroblastic anemia associated with a deletion in the GLRX5 gene (58). The accumulation of iron in mitochondria, which leads to misdistribution of the metal (59) and mismanagement of cellular iron regulatory properties (60, 61), is a hallmark of various diseases. These observations are consistent

with the localization of the FeS cluster biogenesis machinery and key FeS protein metabolic functions in mitochondria (62, 63). Moreover, as mitochondria are the primary energy providers of mammalian cells and key players in a large variety of metabolic processes (62), they have been implicated in metabolic diseases such as type 2 diabetes (33, 64).

Human mNT is composed of two protomers intertwined to form a unique structure with two domains; the β-cap and the cluster binding domain and is the founding member of the NEET fold (12-14, 65). A single-coordinating histidine (H87) and three cysteine ligands (C72, C74, C83) bind the [2Fe-2S] cluster. The single histidine has been shown to effect cluster redox and stability properties (12, 43, 44, 66). Our previous studies on the biophysical properties of the protein led us to investigate whether mNT could serve in FeS cluster transfer. Here we show that mNT transfers its [2Fe-2S] clusters to an apo-acceptor protein. This process occurs only when mNT is in the oxidized state, and mutation of His87 to Cys (H87C) inhibits transfer of the cluster. To assess whether this was a result of the increased cluster stability in the H87C mutant we tested a protein of similar kinetic cluster stability, K55E, and found that it efficiently transfers its [2Fe-2S] cluster to a-Fd. Thus, His87 is critical to efficient cluster transfer. In addition, the transfer rate is orders of magnitude faster than expected from simple release and capture and is quantitative with no apparent loss to degradation that is commonly observed with FeS clusters in solution (17). These results indicate that specific protein–protein interactions between mNT and a-Fd facilitate cluster transfer. As mNT is a target of TZDs we tested its cluster transfer ability in the presence/absence of pioglitazone in

permeabilized human embryonic kidney (HEK293) cells. Pioglitazone inhibits transfer suggesting a possible antidiabetic mode of action for the drug under oxidizing conditions.

EXPERIMENAL METHODS

All the materials used in this work were from best available commercial grade. The acetoxymethyl ester (AM) of calcein green (CalG) was obtained from Molecular Probes. The mitochondrial metal sensor red rhodamine B-[(1,10-phenanthrolin-5-yl) aminocarbonyl] benzyl ester (RPA) was obtained as described elsewhere (67, 68). Pioglitazone (purchased from Shanghai PI Chemicals Ltd.) was dissolved in 100% DMSO and diluted in test medium prior to use.

Expression and Purification of mNT Proteins and a-Fd. The human mNT cDNA encoding the cytoplasmic soluble (mNT) part of the protein (residues 33–108) was amplified by PCR and subcloned into a modified pET28-a(+) vector (Novagen) as described (39). The K55E and H87C mutants of mNT were generated by site-directed mutagenesis of the truncated mNT gene in the bacterial expression vector. The recombinant human mNT and mutant proteins were expressed in Escherichia coli BL21-RIL grown in LB supplemented with 30 μg/mL kanamycin and 34 μg/mL chloramphenicol. At an OD_{600} of 0.6, 0.75 mM $FeCl_3$ was added and cell growth proceeded for additional 18–24 h at 23 °C. From lysed cells, the mNT or mutant proteins were purified using Ni-agarose and size exclusion chromatography as described (39). Purification of a-Fd was performed as described previously (69). Protein concentrations were determined by spectroscopic methods using an extinction coefficient at 280 nm of 9,400 cm^{-1} M^{-1} for mNT and 9,100 cm^{-1} M^{-1} for Fd.

UV-Vis Absorption Spectroscopy, Transfer Kinetics, and Decays. Absorption spectra were recorded at 350–600 nm (CARY, 300Bio), equipped with a temperature control apparatus set to 37 °C. Special attention was given to changes in absorbance at 458 nm (mNT's signature [2Fe-2S] absorbance peak) and at 423 nm (characteristic of the [2Fe-2S] cluster in Fd). The extent of cluster transfer was determined from the ratio R = A423/A458 as shown below:

$$\text{Reaction Progress} = (R_{obs} - R_{initial}) / (R_{final} - R_{initial}) \qquad \text{(Equation 4-1)}$$

In the equation above, R_{obs} is the observed A423⁄A458 ratio at a given time. $R_{initial}$ is the initial A423/A458 ratio at time 0, which is equal to 0.85, and R_{final} is the A423/A458 ratio at long times when the reaction is considered complete and equal to 1.14. Data is normalized and fit to a single exponential rise. Initial transfer rates were determined by taking the tangent of the slope of the fit early into the transfer process (10 min) when concentrations of mNT and a-Fd were still close to their starting amounts. Kinetic measurements were performed using equimolar concentrations of mNT (WT and mutants) and a-Fd in the presence of 50 mM Tris pH 8.0, 100 mM NaCl, 5 mM DTT, and 5 mM EDTA, unless stated otherwise. The a-Fd and DTT were pre-incubated for 30 min prior to the start of the experiment. Decays were performed at 37 °C and determined by monitoring loss of the 458-nm peak with time. Data were then fit to a single exponential. Studies were performed using varying concentrations of mNT in 100 mM citrate 100 mM NaCl for pH < 6.5 and in 100 mM Bis-tris 100 mM NaCl for pH 6.5 and 7.0. As a check for possible buffer or salt effects on decay half-time, experiments at pH 6.0 and 6.5 were performed with both buffers and no significant differences in decay half-time were observed. The log-plotted pH-dependent slopes allowed for extrapolation of cluster decay

times for pH 8.0, which were estimated to take nearly 105 min for WT and 106 minutes for the K55E and H87C mutants.

Native-PAGE [2Fe-2S] Cluster Transfer in Vitro Assay. WT mNT and mutants were incubated (in a rolling shaker) with a-Fd. Both mNT and a-Fd concentrations were 160 μM so that bands could be clearly visualized. The mNT and a-Fd were incubated under vigorous aeration in the presence of 2% β-mercaptoethanol, 5 mM DTT and 5 mM EDTA for the specified time lengths (2.5–60 min). β-mercaptoethanol was added to better keep disulfides reduced because the degree of aeration was higher in the gel assay than in the UV-Vis measurements. Transfer of the [2Fe-2S] cluster from mNT to a-Fd was then analyzed by native-PAGE (70) and checked for completion by UV-Vis spectroscopy.

Labeling of mNT [2Fe-2S] Cluster. $^{55}FeCl_3$ (PerkinElmer, Life Sciences Inc.) was diluted with 100 mM sodium citrate pH 8.0 to 1 μci and incubated with mNT at 1**:**1 ratio (final 2 mM sodium citrate pH 8.0) at 4 °C for a week in a rolling shaker. Following the incubation, mNT was concentrated by centrifugation (4,000 rpm at SS-34 rotor) using a microcon YM-10 (Millipore) filter and washed three times with large excess citrate buffer. Radioactivity was determined on Beckman LS2800 counter (Beckman) and protein labeling was analyzed by native-PAGE and revealed with a phosphor-imager (FujiFilm FLA-3000, Fujifilm Medical Systems).

Cell Culture. Human Embryonic Kidney cells (line HEK293) were grown at 37 °C in 5% CO2 in Dulbecco's modified Eagle's medium (DMEM; Biological Industries) supplemented with 1% antibiotics (penicillin, streptomycin, and amphotericin), 1% glutamine, and 10% fetal calf serum. A day before experimentation, the cells were

washed with PBS and then detached from plates with 1 ml trypsin-EDTA. The cells were diluted to an optimal density of 1–2 million cells per plate (3-cm perforated plate with microscopic slides attached). The cells were further grown for additional 24 h and subjected to epifluorescence imaging on a Zeiss Axiovert 35 (Carl Zeiss) microscope attached to a Polychrome V image system (Till Photonics) (71).

Fluorescence Measurements. HEK293 cells were labeled for 15-min at 37 °C with 1 μM RPA and/or 0.1 μM CalG-AM in DMEM medium containing 10 mM HEPES buffer and supplemented with 10 μM desferrioxamine (DFO) to prevent quenching of the probe by contaminant iron from the medium. After washing with DMEM-HEPES medium and HEPES-buffered saline (HBS) buffer, the cells were permeabilized in HBS buffer pH 7.4 for 180 s with 25 μM digitonin (72). The permeabilized cells were washed with permeabilization buffer (100 mM KCl, 5 mM phosphate buffer, Eagle's MEM-amino acids mix diluted 1:500, 10 mM HEPES, 1 μM $CaCl_2$, 1 mM $MgSO_4$, pH 7.2) and taken to fluorescence microscopy measurements in permeabilization buffer containing 1 mM succinate. For CALG (λ_{exc} 480 nm; λ_{em} 520 nm) and RPA (560 nm excitation-610 nm emission) (73, 74). DFO (1 μM) was present in all solutions during permeabilization and fluorescence measurements, to prevent RPA quenching by contaminant iron. After a 6-min baseline was recorded, 10–50 μM mNT (WT or mutants) was added (with 1 mM DTT) and changes in fluorescence were recorded for 20 min at 37 °C followed by addition of a permeant form of labile iron-FHQ (5 μM FHQ ($FeCl_3$-8-hydroxyquinoline 1:1 complex) so as to attain maximal quenching. The sequences of fluorescent microscopy images were analyzed by the Image J program (National Institutes of Health) (75).

RESULTS

Oxidized mNT, but Not Reduced, Can Transfer Its [2Fe-2S] Cluster to an Apo-Acceptor Protein. We chose a-Fd for cluster transfer experiments because (i) it is the standard for measuring [2Fe-2S] cluster transfer kinetics and (ii) we could take advantage of the fact that Fd has a different ligand environment (4-Cys) than mNT (3-Cys-1-His), leading to a distinguishably different UV-Vis spectrum from which the transfer of mNT's [2Fe-2S] cluster to a-Fd could be easily followed. The UV-Vis spectra of the [2Fe-2S] cluster being transferred changes over time upon mixing of pre-reduced a-Fd and oxidized mNT under oxidizing conditions as it switches its ligand environment. Deconvolution of the overall spectra show the reaction at 10%, 25%, 50%, and 90%completion (Figure 4-1A–D, respectively). These percentages are directly measured from ratio of the peak intensities at 423 nm (Fd) and 458 nm (mNT). Based on initial concentrations of mNTand the final concentration of Fd, we conclude that the [2Fe-2S] cluster transfer was complete and suffers no appreciable loss to solution. This finding was corroborated by native gel electrophoresis (Figure 4-1E, F), followed by colorimetric and ^{55}Fe-labeled [2Fe-2S] detection (Figure 4-1F). Holo-mNT's red-colored band intensity decreased over time when incubated with a-Fd, and the latter is concomitantly converted to the red-colored holo-Fd band. The levels of mNT and a-Fd/Fd remained unchanged as shown by Coomassie staining (Figure 4-1E). UV-Vis-monitored cluster transfer experiments show that [2Fe-2S] cluster transfer readily occurs under oxidizing

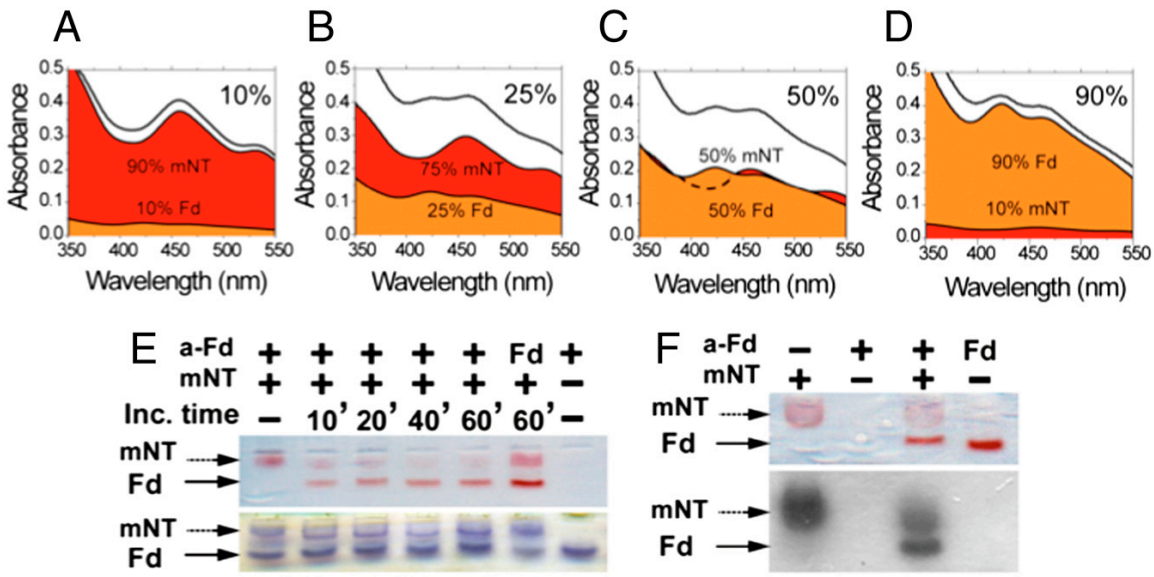

Figure 4-1: Facile transfer of the [2Fe-2S] cluster from mNT (mNT) to apo-ferredoxin (a-Fd). The presence of the [2Fe-2S] cluster in mNTcan be observed by UV-Vis spectroscopy with a signature peak at 458 nm and in Fd at 423 nm. Frames A through D show the cluster transfer reaction progress. The observed spectra for the combined species are shown as a black line at the top of each frame while the deconvoluted spectra of holo-mNT (red) and holo-Fd (orange) are shown below. (D) Upon approaching completion, the visible spectrum resembles that of Fd, as all a-Fd has been converted to the holo form and mNT has been converted to the visible-lacking apo form. The upper right corner in each spectrum indicates the percent completion for the cluster transfer reaction. (E) Transfer of mNT's [2Fe-2S] cluster to a-Fd is also observed by native-PAGE. Upon incubation with a-Fd, mNT shows diminished color, indicating cluster loss over time as the [2Fe-2S] cluster is transferred to a-Fd and the presence of a smaller molecular weight red-colored band indicating formation of holo-Fd. (F) In addition, ^{55}Fe-labeled mNT was shown to transfer its cluster to a-Fd by native-PAGE and radioactivity detection. UV-Vis and Native-PAGE cluster transfer experiments were performed at 37 °C using 160 **µ**M a-Fd and 160 **µ**M mNT in the presence of 50 mM Tris pH 8.0, 100 mM NaCl and 5 mM DTT (29).

conditions as both the initial mNT spectra (Figure 4-1A), and final Fd spectra (Figure 4-1D), reflect those of each of the respective oxidized species. As mNT's cluster binding domain on the outer mitochondrial membrane is believed to face the cytosol, we wanted to see if transfer was inhibited under reducing conditions like those normally found in this cellular environment. Because both oxidized and reduced mNT have distinct spectra both from each other and Fd we could follow transfer both under oxidizing as well as reducing conditions. Reduced mNT shows no cluster transfer to a-Fd over a period of 500 min (Figure 4-2A). Upon addition of oxygen mNT becomes oxidized, as seen by the characteristic oxidized spectra (Figure 4-2B) and readily transfers its [2Fe-2S] cluster to a-Fd (Figure 4-3). These results show that mNT's oxidation state regulates whether it can transfer its cluster to a-Fd, and that this cluster transfer capability may normally be inhibited in the reduced cytosolic environment.

His87 Is Critical for Cluster Transfer Between mNT and a-Fd. A projection of mNT's cluster binding site shows the rare 3-Cys-1-His (Fig. 4-4A). We replaced the coordinating His87 with Cys (H87C) to test the role of this residue in cluster transfer. In addition, we replaced Lys55 with Glu (K55E) because this change dramatically alters the properties of the cluster (43).

Time-dependent spectroscopic changes measured by UV-Vis absorption spectroscopy allowed us to quantitatively measure the rate of cluster transfer for WT mNTand the K55E and H87C mutants. Cluster transfer is slowed only slightly in the K55E mutant whereas the transfer rate was significantly retarded by replacement of the single-coordinating His87 with Cys (Figure 4-4B, C and Table 4-1). The cluster transfer rates are distinct from passive decay because (i) the transfer rate to a-Fd is concentration

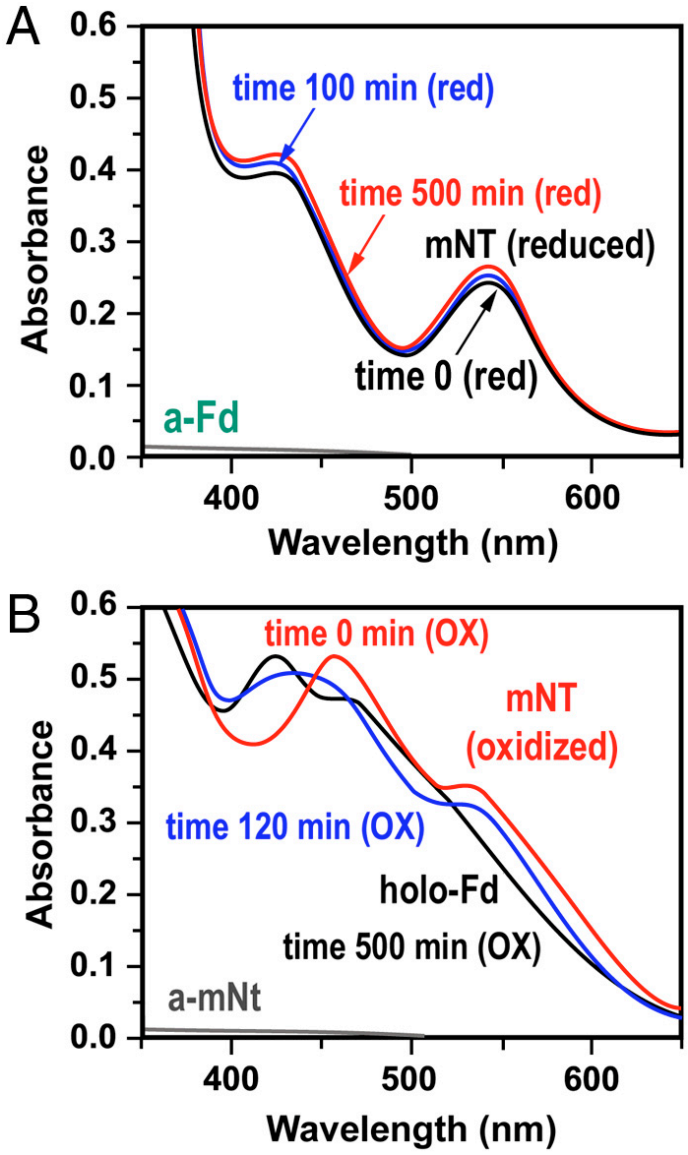

Figure 4-2: UV-Vis absorption spectroscopy shows that mNT does not transfer its cluster under reducing conditions. (A) Initial black trace shows reduced mNT spectra due to presence of excess DTT. After 100 minutes (blue trace) and 500minutes (red trace) spectra still resembles that of reduced mNTalone (black trace). The apo-Fd (a-Fd) does not have an absorption in the visible region and is shown in gray. (B) Oxidation of mNT (red trace) confirms that spectrum resembles that of mNTand no significant transfer occurred in 500 minutes prior to oxidation. Absorption spectra 120 minutes after oxygen was added (blue) and 500 minutes afterwards (black) show facile transfer of mNT's [2Fe-2S] cluster to a-Fd. The apo-mNT (a-mNt) does not have an absorption in the visible region and is shown in gray (29).

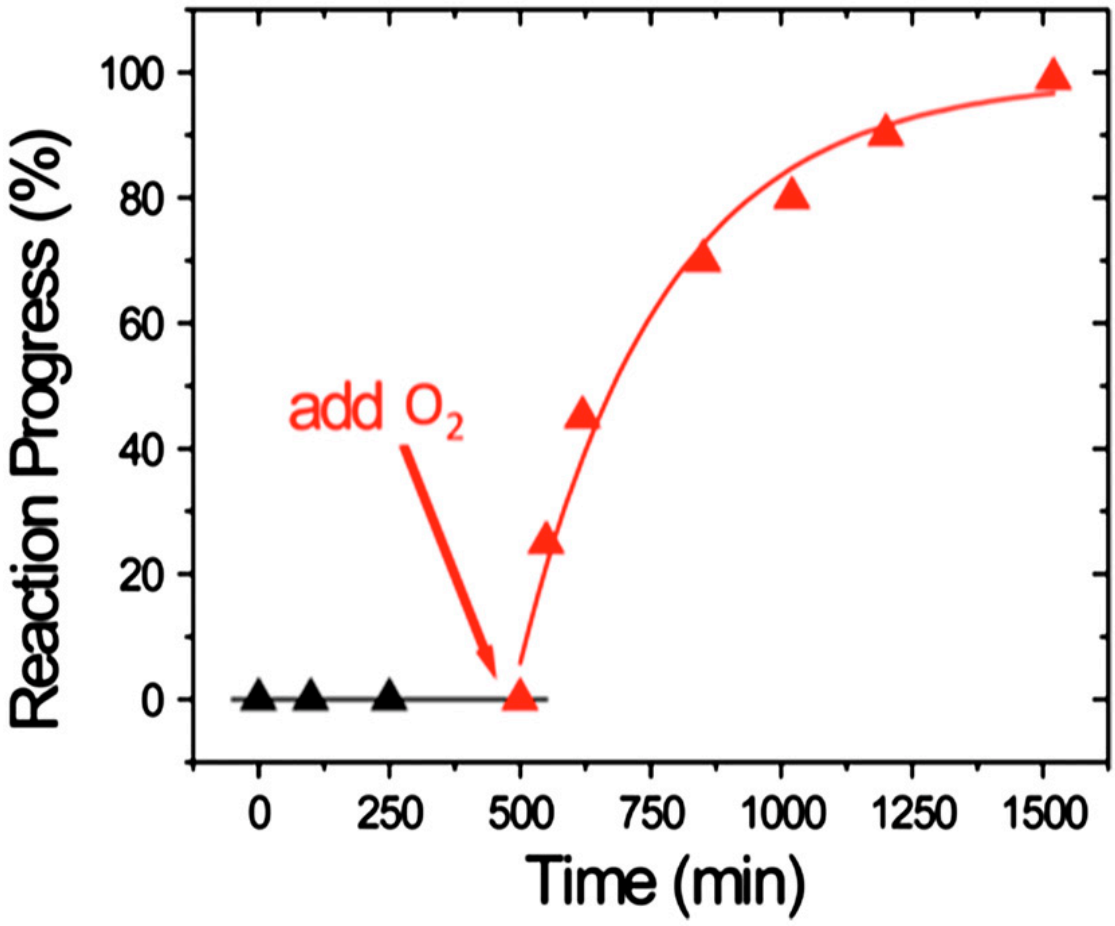

Figure 4-3: Facile cluster transfer from mNT to a-Fd occurs only under oxidizing conditions. No reaction progress (i.e., changes in visible spectrum) occurs even after 500 minutes under reducing conditions (black triangles). Upon addition of oxygen to reaction the visible absorption spectrum shifts to that of oxidized mNT (red triangles) and cluster transfer is observed over time. UV-Vis kinetic trace was obtained at 37 °C using 80 **µ**M a-Fd and 80 **µ**M mNT in the presence of 50 mM Tris pH 8.0, 100 mM NaCl and 50 mM DTT (29).

dependent (Figure 4-5A), whereas passive decay is not (Figure 4-5B), and (ii) the transfer rate is many orders of magnitude faster than passive cluster release (Table 4-1), hence the reaction is catalyzed. We observed no correlation between kinetic cluster stability and cluster transfer rate because the K55E shows transfer rates similar to WT mNT (Table 4-1), yet its kinetic cluster stability is similar to that of the H87C mutant (Table 4-1 and Figure 4-6). The observed cluster transfer rate for mNT is protein concentration dependent with a measured rate constant of 185 ± 11 M^{-1} min^{-1}, a rate constant similar to the well-characterized FeS transfer protein ISA (170 M^{-1} min^{-1}, Table 4-1) (76).

The Diabetes Drug Pioglitazone Inhibits Iron Transfer from mNT into the Mitochondria. Having demonstrated that mNT can transfer its [2Fe-2S] cluster to an apo-acceptor, we asked if it could be a source of free iron in cells. We used cytosolic and mitochondrial fluorescent indicators to assess changes in free iron levels upon introduction of mNT. We used gently permeabilized HEK293 cells that were double labeled with the fluorescent iron sensors calcein-green (CALG) as tracer for the cytosolic iron, and red rhodamine B-[(1,10-phenanthrolin-5-yl)-aminocarbonyl] benzyl ester (RPA) as a tracer for iron in the mitochondrial matrix (Figure 4-7A). We show changes in fluorescence in response to the addition of mNT (Figure 4-7B). Quenching of RPA, but not CALG, occurred rapidly and was directly proportional to mNT's concentration (Figure 4-7C) indicating transfer of iron to the mitochondrial matrix. Pre-incubation of mNT with a-Fd prevented iron transfer into mitochondria (Figure 4-7D). We tested the importance of increased cluster stability introduced by mutation or drug binding to iron transfer in the cellular system. The K55E mutant is equivalent to the wild type for iron

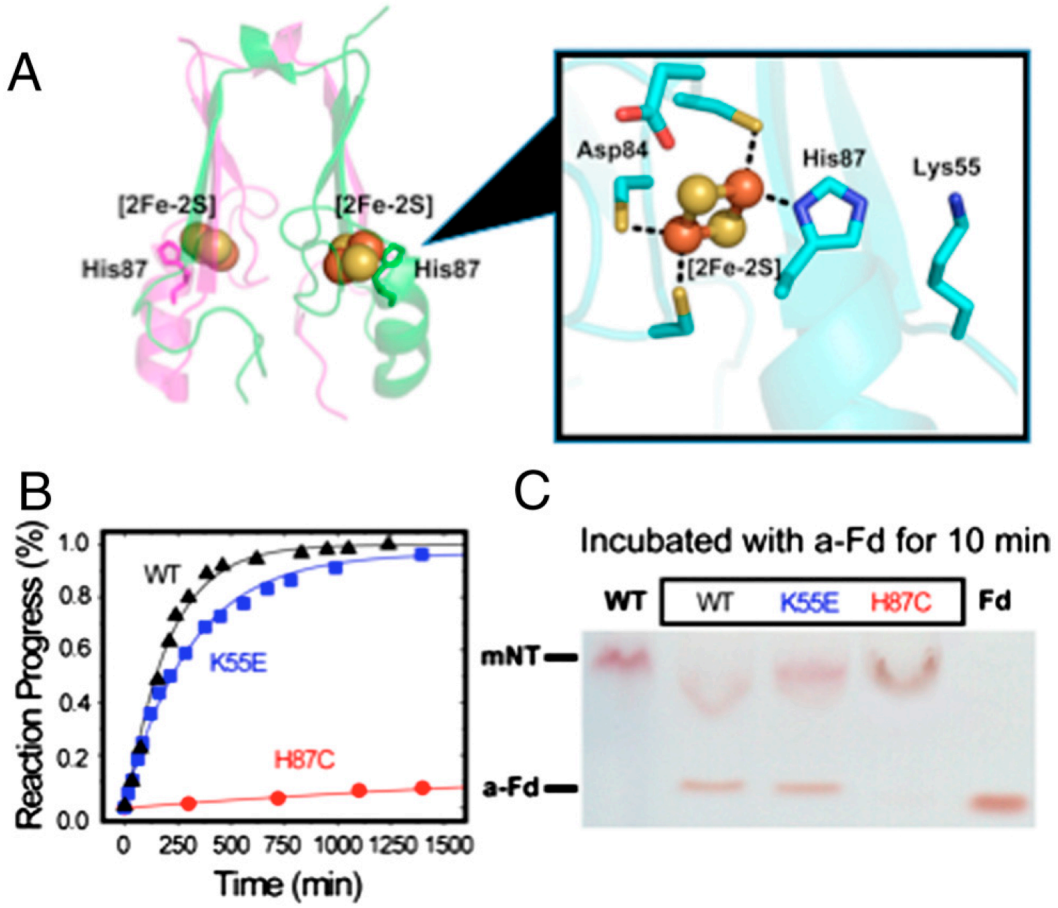

Figure 4-4: Cluster transfer is inhibited in the 4-Cys mutant (H87C). (A) Each [2Fe-2S] cluster in mNT is ligated by 3-Cys-1-His. The cluster binding site shows directly coordinating Cys and His ligands as well as additional local residues that may play key role in cluster transfer. (B) UV-Vis absorption spectroscopy kinetics were used to monitor transfer of the [2Fe-2S] in mNT and two mutants: K55E and H87C, to a-Fd. Cluster transfer remains relatively unchanged in the K55E but significantly hindered in the H87C mutant. The cluster transfer reaction for WT mNT (black triangles) shows 50% completion (A423/A458 . 0.5) in 120 min, the K55E mutant (blue squares) requires 220 min, and the H87C (red circles) requires >10;000 minutes. UV-Vis experiments were performed at 37 °C using 80 µM mNT, 80 µM a-Fd (incubated in 5 mM DTT for 30 min prior to use) in the presence of 50 mM Tris pH 8.0, 100 mM NaCl, and 5 mM EDTA. (C) WT mNT and mutant proteins (160 µM, higher protein concentrations are needed for visualization) were incubated with a-Fd for 10 min under similar conditions, followed by native-PAGE. The red-colored upper bands indicate WT mNT and mutant proteins while the lower red bands indicate presence of holo-Fd, bearing the [2Fe-2S] cluster from mNT. The results indicate His87 is critical for cluster transfer to an a-Fd acceptor (29).

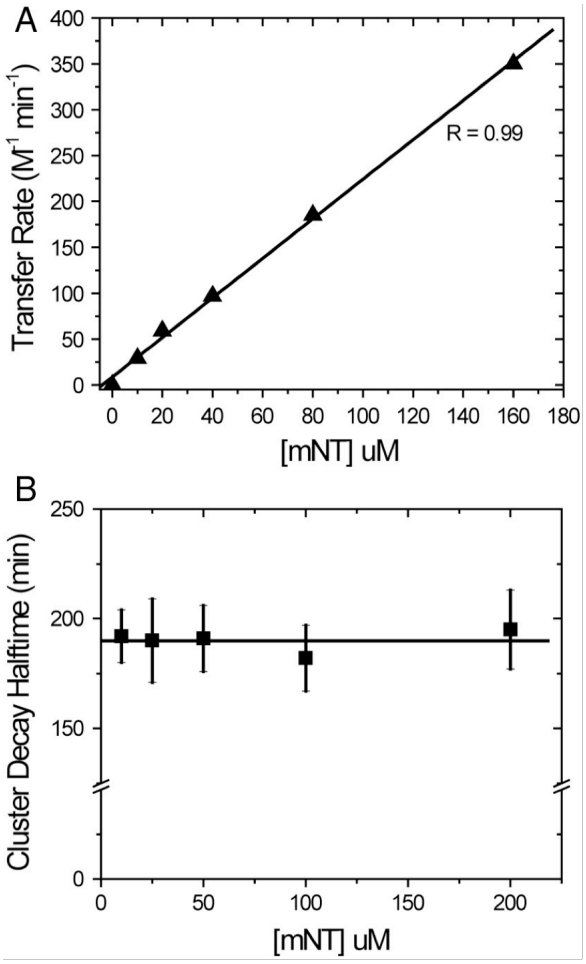

Figure 4-5: Cluster transfer rates are concentration dependent. (A) Concentration dependence on the [2Fe-2S] cluster transfer rate to a-Fd. All experiments were done with varying [mNT] and 160 μM a-Fd. Transfer experiments show linear relationship between [mNT] and reaction rate. In addition to varying concentrations of mNT all reactions included 80 μM a-Fd preincubated with 5 mM DTT in 100 mM NaCl, and 5 mM EDTA. All experiments were performed at 37 °C and transfer rates were determined as described in Experimental Methods. (B) Non-catalyzed cluster decay process as a function of [mNT]. Measurements were performed by monitoring loss of 458 nm peak characteristic of mNT's [2Fe-2S] cluster over time. Data were fit to a single exponential and decay half-times were plotted versus concentration of mNT. Decays were performed here at pH 6.0 in 100 mM citrate 100 mM NaCl (29).

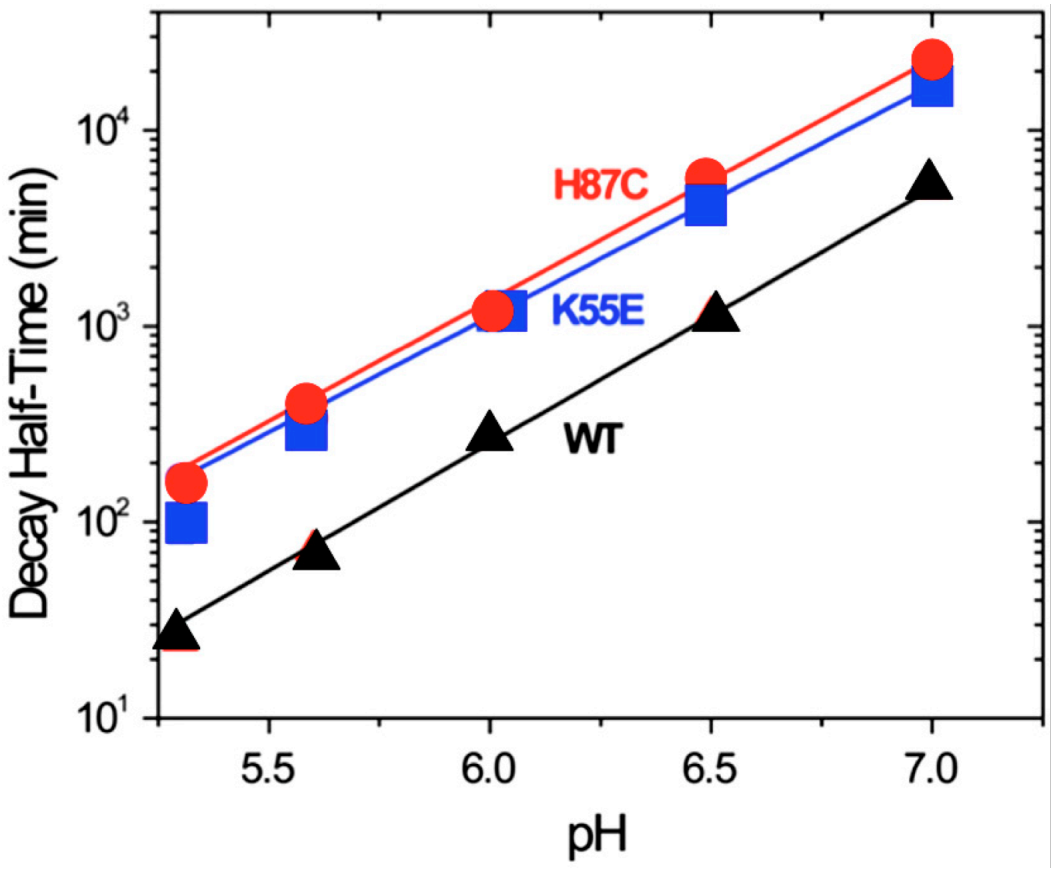

Figure 4-6: Monitoring [2Fe-2S] cluster decay for WT mNT and mutants as a function of pH. Both the WT and the two mutants have a similar pH-dependence to their kinetic cluster stabilities. The kinetic cluster stability of the WT (black) is approximately 10-fold less than the K55E (blue) and H87C (red). Decays shown here were done at 37 °C and determined by monitoring loss of the 458 nm peak with time. Data was then fit to a single exponential and plotted against time using a log scale. Decay studies were performed using 50 **µ**M protein in 100 mM citrate 100 mM NaCl at varying pH. Measurements at pH 7.0 were performed using 100 mM Bis-tris 100 mM NaCl instead. Decay measurements at pH 6.0 and 6.5 were performed using either 100 mM Bis-tris or 100 mM citrate along with 100mMNaCl and no differences in decay time were observed. The slopes allow for extrapolation of cluster decay times for pH 8.0 for use in Table 4-1, which are estimated to take nearly 105 min for WT and 106 minutes for K55E and H87C (29).

Table 4-1: Comparison of mNT cluster transfer rates with mutants and ISA.

	Cluster decay half-time (min^{-1})	Initial transfer rate (M^{-1}, min^{-1})	Transfer rate at 160 μM [mNT] (min^{-1})	Catalytic enhancement of transfer rate at 160 μM [mNT] (lower limit)
WT	10^{-5}	185 ± 11	0.03	3×10^3
K55E	10^{-6}	115 ± 4	0.02	10^4
H87C	10^{-6}	<1	NA	NA
ISA*	NA	170 ± 8	NA	NA

*Experiments performed at 25 °C on Iron-sulfur cluster assembly protein (ISA).

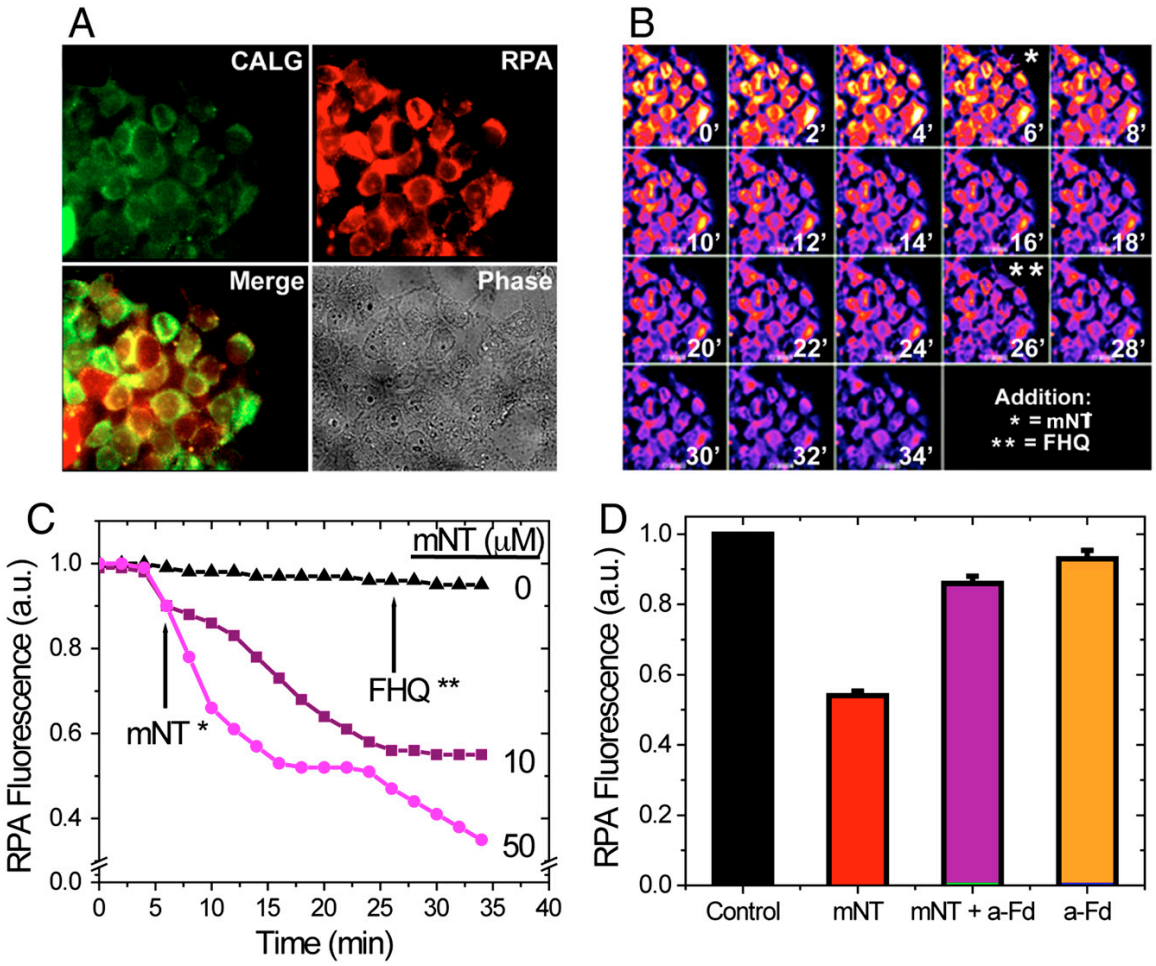

Figure 4-7: Transfer of [2Fe-2S]/Fe from mNT to mitochondria in permeabilized HEK293 cells. HEK293 cells labeled with iron sensors RPA (for mitochondria) and calcein-green (CALG) (for cytosol) were permeabilized (A) and used for tracing changes in fluorescence (B and C) following addition of mNT in succinate medium. (B) A time series of fluorescence pseudocolor images; RPA fluorescence intensity is given in arbitrary units (a.u.) following addition of 50 μM mNT and FHQ (6 μM) at different times (indicated by * or ** respectively). (C) The fluorescence traces (reported as a.u.) represent time series taken for cells exposed to different concentrations of mNT. (D) RPA fluorescence 20 minutes after the addition of 10 μM mNT under different conditions. The black bar represents a fluorescent trace from control cells where no additions were made. The red bar represents the fluorescence of cells after mNT addition, the purple bar shows the addition of mNT. In this experiment a-Fd is pretreated with DTT to reduce the free cysteines and prevent inter-disulfides. After 30 min the free DTT is depleted at which point mNT is added. The orange bar represents the fluorescence of cells after addition of a-Fd only. All data are represented as mean ± standard error (SE). The statistical differences between treatments were determined by the paired t test at significance levels * $p < 0.05$ or ** $p < 0.01$. (N = 14) (29).

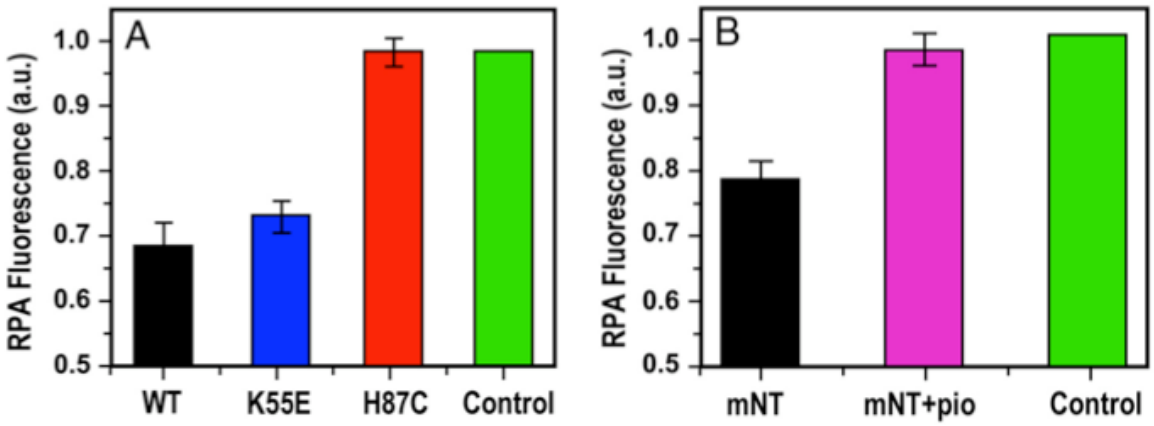

Figure 4-8: Transfer of [2Fe-2S]/Fe from mNT's mutants to permeabilized HEK293 cells labeled with RPA. (A) RPA fluorescence was measured 20 min after the addition of 10 μM of WT mNT or mutants: WT mNT (black), K55E (blue), and H87C (red) bar, respectively. The green bar represents a fluorescence trace from control cells with no additions. Data are represented as mean ± standard error (SE). (N = 17). (B) The anti-diabetic drug, pioglitazone inhibits the Fe/Fe-S transfer from mNT to mitochondria in permeabilized HEK293 cells. Permeabilized cells loaded with RPA were examined by fluorescence microscopy as previously described. The data represent RPA levels 20 min after the addition of: 10 μM mNT (black bar), mNT (10 μM) pre-incubated with pioglitazone (100 μM), noted as mNT+pio, (purple bar), and a fluorescence trace from control cells with no additions (green bar). Data are represented as mean ± standard error (SE). The statistical differences between treatments were determined by paired t test at significance levels $p < 0.01$. (N = 4) (29).

transfer to the mitochondria whereas H87C mutant inhibits transfer (Figure 4-8A). Importantly, the addition of pioglitazone to WT inhibited iron transfer (Figure 4-8B), indicating a PPARγ-independent effect of TZDs.

DISCUSSION

The rare 3-Cys-1-His ligation geometry of the [2Fe-2S] cluster of mNT (12-14, 81) is only observed in a few other cases, notably in a mutant version of the FeS cluster transfer protein IscU (77), and because the role of IscU is important in FeS cluster assembly we investigated whether mNT can perform cluster transfer. In order to assess this hypothesis, we examined the cluster transfer potential of mNT using a-Fd, a universal acceptor protein used in FeS studies (76). We demonstrate that mNT's [2Fe-2S] cluster is transferable to a-Fd (Figure 4-1A–F) at a rate constant (185 ± 11 M^{-1} min^{-1}) equivalent to the cluster transfer protein ISA (170 ± 8 M^{-1} min^{-1}) (76). In addition, we find that replacement of the single His ligand to Cys inhibits the process, emphasizing the importance of this coordination in efficient transfer.

We also show that increased levels of mNT lead to Fe accumulation in mitochondria as reported by RPA fluorescent quenching assays in HEK293 cells (Figure 4-8A). Fe accumulation is observed with the K55E mutant but not with the H87C mutant protein. Because K55E and H87C have similar cluster stabilities it is clear from this data that His87 is an essential mediator of cluster transfer in cells. The fact that Fe accumulates in the mitochondrial matrix suggests there is a means by which mNT, tethered to the outer mitochondrial membrane, transfers Fe into the matrix. The mechanism in vivo is currently under investigation. Taken together, our findings in the

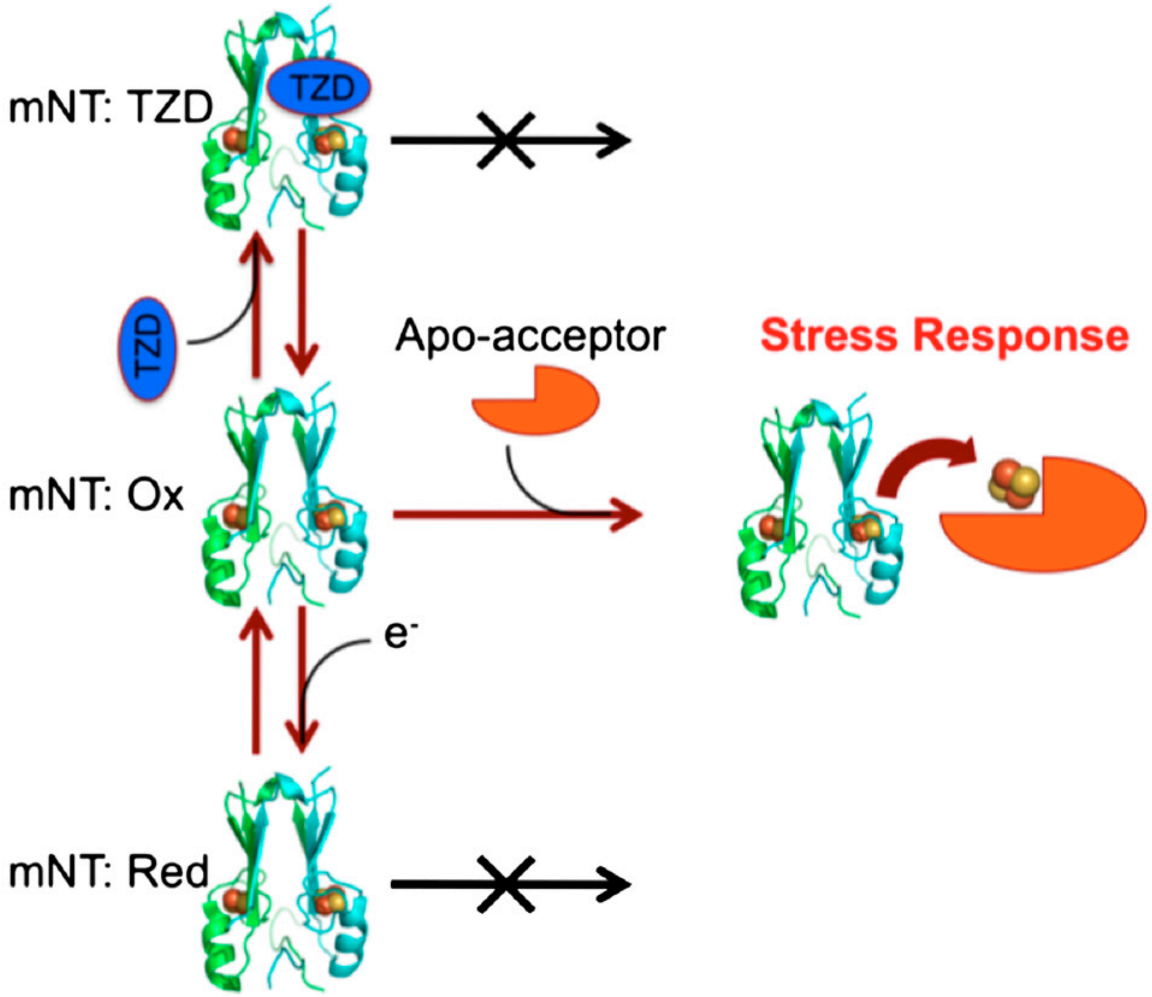

Figure 4-9: Model describing a possible therapeutic mode of action for TZDs like pioglitazone. The cytosol is normally highly reducing (38), which suggests that mNT is predominantly in the reduced state under normal cellular conditions. Changes to the cytosolic redox potential, which occur when cells are under oxidative stress, could induce transfer of mNT's [2Fe-2S] cluster. If not carefully regulated, this could lead to Fe overload stress, which is a problem in patients with type 2 diabetes. Pioglitazone, which shows a strong preferential binding to mNT in the oxidized state (28), may act to alleviate this stress (29).

cellular system, which are similar to that observed in vitro, underscore the fact that the conserved His87 ligand facilitates transfer.

TZD cross-linking studies led to the discovery of the mitochondrial drug target, mNT (9). This target is completely distinct from the accepted paradigm protein, the nuclear transcription factor PPARγ. Here, we report the direct effect of TZD binding to mNT in cellular systems. We show that pioglitazone is capable of regulating Fe accumulation in mitochondria in this study. In addition to providing a cellular readout for TZD binding, this data provides a direct link between previous in vitro observations and our current in vitro and cellular findings. We now present a model describing a possible therapeutic mode of action for pioglitazone (Figure 4-9). As the cytosol is normally a highly reducing environment (38), mNT is expected to be found predominantly in its reduced state. Changes to the cytosolic redox potential, which occur when cells are under oxidative stress (35), could induce transfer of mNT's [2Fe-2S] cluster. If not carefully regulated, this could lead to Fe overload stress, which is a problem in patients with type 2 diabetes (78). Pioglitazone, which shows a strong preferential binding to mNT in the oxidized state (28), may act to alleviate this stress.

CONCLUSIONS

We show that oxidized mNT transfers [2Fe-2S] clusters readily and efficiently, and that reduction of the cluster inhibits transfer. In addition, we show that the hallmark His87 ligand is a critical player in facilitating cluster transfer and provide direct evidence for a functional effect of TZD binding to this protein in cells. Our findings raise a set of interesting questions about this class of [2Fe-2S] proteins. Notably, do mNT proteins play a role in [2Fe-2S] cluster transfer along with the mitochondrial iron-sulfur cluster

assembly (ISC) (17) or cytosolic iron-sulfur cluster assembly (CIA) machinery (79), as mNT's unique position on the outer mitochondrial membrane suggests it could be useful as a conduit between the cytosol and the mitochondria? Is mNT an [2Fe-2S]/Fe reservoir that provides clusters upon demand? It is possible that mNT acts as a redox sensor and transfers its cluster only when in the oxidized state, such as when cells are stressed. It was long assumed that the TZD class of anti-diabetes drugs acted only in a PPARγ-mediated fashion. Because pioglitazone inhibits this biochemical process it is clear that determining mNT's protein partners and a better understanding of how the protein–drug interaction relates to alleviating the negative effects of type 2 diabetes will be of great importance in the future.

Chapter 4, in part, is a reprint of the material that appears in Proceedings of the National Academy of Sciences by Zuris JA, Harir Y, Conlan AR, Shvartsman M, Michaeli D, Tamir S, Paddock ML, Onuchic JN, Mittler R, Cabantchik Z-I, Jennings PA, Nechushtai R. 108 2011. The dissertation/thesis author was the primary investigator and author of this paper.

Chapter 5

NADPH Inhibits [2Fe-2S] Cluster Protein Transfer from Diabetes Drug Target MitoNEET to an Apo-acceptor Protein

ABSTRACT

MitoNEET (mNT) is the founding member of the recently discovered CDGSH family of [2Fe-2S] proteins capable of [2Fe-2S] cluster transfer to apo-acceptor proteins. It is a target of the thiazolidinedione (TZD) class of anti-diabetes drugs whose binding modulate both electron transfer and cluster transfer properties. The [2Fe-2S] cluster in mNT is destabilized upon binding of NADPH, which leads to loss of the [2Fe-2S] cluster to the solution environment. Because mNT is capable of transferring [2Fe-2S] clusters to apo-acceptor proteins, we sought to determine whether NADPH binding also affects cluster transfer. We show that NADPH inhibits transfer of the [2Fe-2S] cluster to an apo-acceptor protein with an inhibition constant (K_i) of 200 μM, which reflects that of NADPH concentrations expected under physiological conditions. In addition, we determined that the strictly conserved cluster interacting residue Asp84 in the CDGSH domain is necessary for the NADPH-dependent inhibition of [2Fe-2S] cluster transfer. The most critical cellular function of NADPH is in the maintenance of a pool of reducing equivalents, which is essential to counteract oxidative damage. Taken together, our findings suggest that NADPH can regulate both mNT [2Fe-2S] cluster levels in the cell as well as the ability of the protein to transfer [2Fe-2S] clusters to cytosolic or mitochondrial acceptors.

INTRODUCTION

Human mNT (mNT) is a newly discovered FeS-containing protein that is a target (9) of the insulin-sensitizing thiazolidinedione (TZD) class of type 2 diabetes drugs (52, 53). The interaction of TZD drugs with mNT has been proposed to be of therapeutic importance (9). This is the first FeS protein to be directly targeted by drug binding (12). Crystallization of human mNT revealed that the protein contains two [2Fe-2S] clusters (12-14) (Figure 5-1), which are more labile than typical [2Fe-2S] cluster-containing proteins (11). TZD binding to mNT both stabilizes the [2Fe-2S] cluster against release (12) and shifts the redox potential by as much as 100 mV (28). Recently, we discovered that mNT is a cluster transfer protein both in vitro and in vivo (30). TZD binding blocks iron transfer/overload in mitochondria (29). Because NADPH binding was recently found to destabilize the [2Fe-2S] cluster in mNT (80), it poses an interesting question: does NADPH binding alter the cluster transfer or redox properties of mNT?

In this study we used the unique visible spectrum of the [2Fe-2S] cluster inmNTto investigate interactions between the protein and NADPH. We found that NADPH inhibits transfer of the [2Fe-2S] cluster in mNT to an apo-acceptor protein, in this case apo-ferredoxin (a-Fd), at concentrations typically found incells. We also found that NADPH binding causes a negative shift in the redox potential of mNT in a manner similar to the TZDs, suggesting involvement of His87 in NADPH binding. Finally, we found that the conserved Asp84 in the CDGSH domain is essential for inhibition of cluster transfer by NADPH, which suggests a role for the strict conservation of this residue across CDGSH family members. Taken together, these findings suggest a potential role for NADPH as a cellular regulator of the [2Fe-2S] cluster transfer from mNT to apo-acceptor proteins.

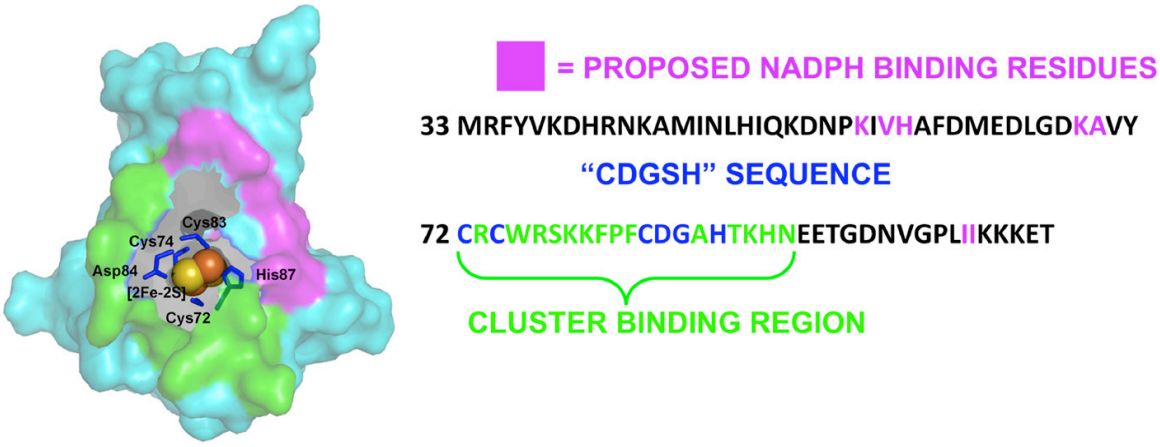

Figure 5-1: Proposed NADPH binding site. Surface representation of mNT structure (Protein Data Bank code 2QH7) is shown in gray with [2Fe-2S] cluster as red and yellow spheres. The unusual 3-Cys-1-His ligand coordination found in mNT is shown as blue sticks. Asp84, part of the CDGSH domain, is shown as well (blue sticks). Residues that show chemical shift changes upon binding of NADPH (80) are shown in magenta. Cluster binding region is shown as a green surface. The sequence (amino acids 33–108) of the mNT construct used in this study is shown to the right (30).

EXPERIMENTAL METHODS

Protein Expression and Purification. Overexpression and purification of the soluble fragment of mNT (amino acids 33–108) as well as a-Fd were performed as outlined previously (39).

Optical Spectroscopy, Cluster Transfer Kinetics, Potentiometric Redox Titrations, and Cluster Stability Measurements. All UV-visible absorption spectra were measured from the near UV to the near IR (300–800 nm) on a Cary50 spectrophotometer (Varian, Palo Alto, CA) equipped with a temperature-controlled cell. The methods employed in this study for monitoring cluster transfer kinetics are identical to those reported previously on mNT (29). Further details on experimental conditions used in FeS cluster transfer studies can be found in Wu and Cowan (76). In this study, cluster transfer experiments were performed aerobically at 35 °C at pH 8.0 with and without varying concentrations of NADPH (Fisher Scientific) using 100 μM mNT or D84S mutant and 100 μM a-Fd in 50 mM BisTris, 100 μM NaCl. The samples were covered with mineral oil (Hampton Research) to prevent losses due to evaporation. Transfer rates were obtained by following the (423 nm)/(458 nm) ratio corresponding to loss of the mNT 458 nm peak and emergence of the holo-ferredoxin 423-nm peak with time as described previously (29). Data were fit to a single exponential decay, and transfer rates were determined by taking the slope of the exponential fit after the first 15 min. Transfer rates were then fit to a standard Michaelis-Menten curve.

$$\text{Rate} = \frac{V_{max}}{1 + \frac{[\text{NADPH}]}{K_i}} \qquad \text{(Equation 5-1)}$$

In the equation, V_{max} is the maximum transfer rate in the presence of 100 μM mNT and a-Fd in the absence of any NADPH (measured to be 225 M^{-1} min^{-1}), and K_i is the inhibition constant for the inhibitor NADPH. A detailed explanation of optical potentiometric redox titration methods can be found elsewhere (40). For this study, optical potentiometric redox titrations were performed as outlined previously (43) but with the addition of 10 mM NADPH where noted. Briefly, experiments were performed anaerobically at 25 °C under an argon atmosphere with and without 10 mM NADPH using 50 μM mNT in 50 mM BisTris, 50 mM Tris, 100 mM NaCl (to span the pH range 6.0–9.0) at varying pH values in the presence of mediators. Sodium dithionite (Sigma-Aldrich) was titrated in via syringe to reduce the [2Fe-2S] clusters, and once fully reduced, mNT was reoxidized by titrating in fixed amounts of ambient oxygen through a syringe. Optical scans (300–700 nm) were performed with each addition of dithionite or oxygen. Optical potentiometric redox titration data were fit to the Nernst equation, and redox potentials were plotted as a function of pH as described previously (43). From this fit the variables pK_{ox} and E_{acid} could be determined in the presence and absence of NADPH.

Cluster stability measurements were performed aerobically at 35 °C at pH 6.0 using 50 μM D84S or H87C mutant with and without 10 mM NADPH in 100 mM Bis-Tris, 100 mM NaCl. Cluster loss was measured as a decrease in absorbance at 458 nm.

RESULTS

NADPH Inhibits Transfer of [2Fe-2S] Clusters from mNT to an Apo-acceptor Protein. NADPH is the first identified physiological coenzyme that binds to mNT (26), as recently shown by measuring NMR chemical shift perturbations in specific

residues in mNT in the presence of NADPH (80). However, NMR methods are not easily amenable to monitor the FeS cluster directly because of the paramagnetic broadening of residues surrounding the cluster (Figure 5-1). To determine whether NADPH binding affects [2Fe-2S] cluster transfer of to an acceptor protein (29) we tested for cluster transfer in the presence of NADPH. NADPH inhibits transfer of the [2Fe-2S] cluster to a-Fd in a concentration- dependent manner (Figure 5-2A). Fitting a standard Michaelis-Menten curve to the data (Figure 5-2B) yields an inhibition constant (K_i) equal to 200 ± 60 μM. This value falls within the expected physiological concentration of NADPH, which varies between different organisms as well as different human tissues but is estimated to be between 100-200 μM (81, 82).

Binding of NADPH Leads to Shift in the pH-dependent Redox Potential. In this work we used visible spectroscopy (Figure 5-3A) to determine the effect of the coenzyme on mNT cluster properties (43, 44, 65, 66, 83) such as redox potential. In addition, we tested the coenzyme sensitivity of mutant mNT in which mutations were made in the CDGSH domain (Figure 5-3B). Upon addition of excess NADPH, mNT is not reduced, even after a 25-h incubation (Figure 5-3A, blue line). No reduction of the [2Fe-2S] cluster is observed even though the redox potential for NADPH is -320 mV, which is significantly lower than that of the [2Fe-2S clusters] of mNT (~0 mV) (28). Thus, the reduction of mNT is clearly kinetically inhibited. To determine whether binding of NADPH affects the redox potential of mNT, we performed optical potentiometric titrations (43) on the protein in the presence of 10 mM NADPH and mediators (Figure 5-3C). We observed a decrease in redox potential of ~ 40 mV at pH 6.0. As a control we found that redox changes were not observed in the presence of NADH (Figure 5-3D),

which does not bind mNT (80). Thus, the additional phosphate group of NADPH is essential for the binding of NADPH to mNT.

Because the redox properties of mNT are pH-dependent (28) we wished to explore whether NADPH binding affects the pH profile. The pH-dependent redox potential of the [2Fe-2S] cluster in mNT can be adequately described as being coupled to a single titrating group. Two terms describe the pH-dependent redox potential for mNT; they are E_{acid} and pK_{ox}, which have been described in more detail previously (43). Briefly, E_{acid} is the redox potential of the protein when a single redox-coupled group is in the fully protonated state, whereas pK_{ox} is the pH at which the redox-coupled group is half protonated. E_{acid} for mNT was previously shown to be +40 mV and pK_{ox} to be 6.8.

The redox-coupled group which undergoes protonation upon reduction of the [2Fe-2S] cluster was attributed to the non cluster-coordinating N-ε of His87 (43). The redox shift for mNT in the presence of NADPH is more dramatic at pH <7.0 and less so at pH >7.0 (Figure 5-4, black and white circles), indicating that binding of NADPH shifts pK_{ox} from pH 6.8 to pH 7.8. It is also clear that E_{acid} has been shifted -40 mV (Figure 5-4). We attribute this negative change in E_{acid} to the addition of multiple negative charges from the phosphate groups of NADPH. Placement of a negative charge near the [2Fe-2S] cluster should discourage the further addition of negative charge resulting from a single electron reduction, which consequently results in a lower measured value for E_{acid}. Having previously proposed that pK_{ox} is due to protonation of His87 (43), these results suggest that binding of NADPH either directly or indirectly involves His87.

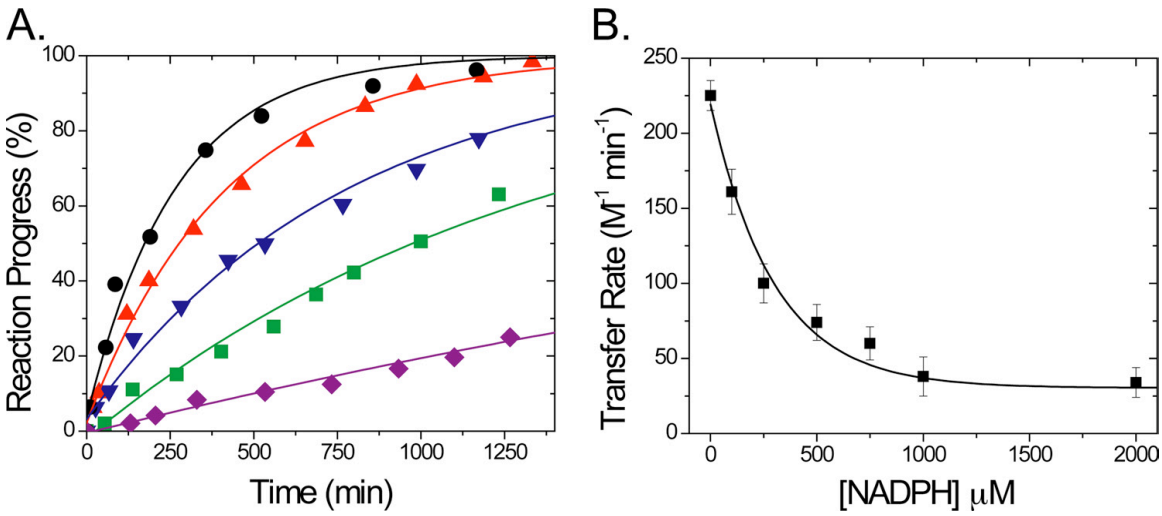

Figure 5-2: Binding of NADPH inhibits transfer of [2Fe-2S] cluster from mNT to a-Fd. A, oxidized mNT was incubated with a-Fd, and cluster transfer was observed with time as reported previously (29) (black circles). To test the effect of NADPH on the cluster transfer rate, oxidized mNT was incubated with a-Fd and varying concentrations of NADPH: 0.1 mM (red triangles), 0.5 mM (blue triangles), 1 mM (green squares), and 10 mM (purple diamonds). Cluster transfer experiments were performed at 35 °C at pH 8.0 with and without varying concentrations of NADPH using 100 μM mNT and 100 μM a-Fd in 50 mM Tris, 100 mM NaCl. B, cluster transfer rates were plotted as a function of NADPH concentration. Rates were fit to a Michaelis-Menten curve, giving inhibition constant (K_i) = 200 ± 60 μM (30).

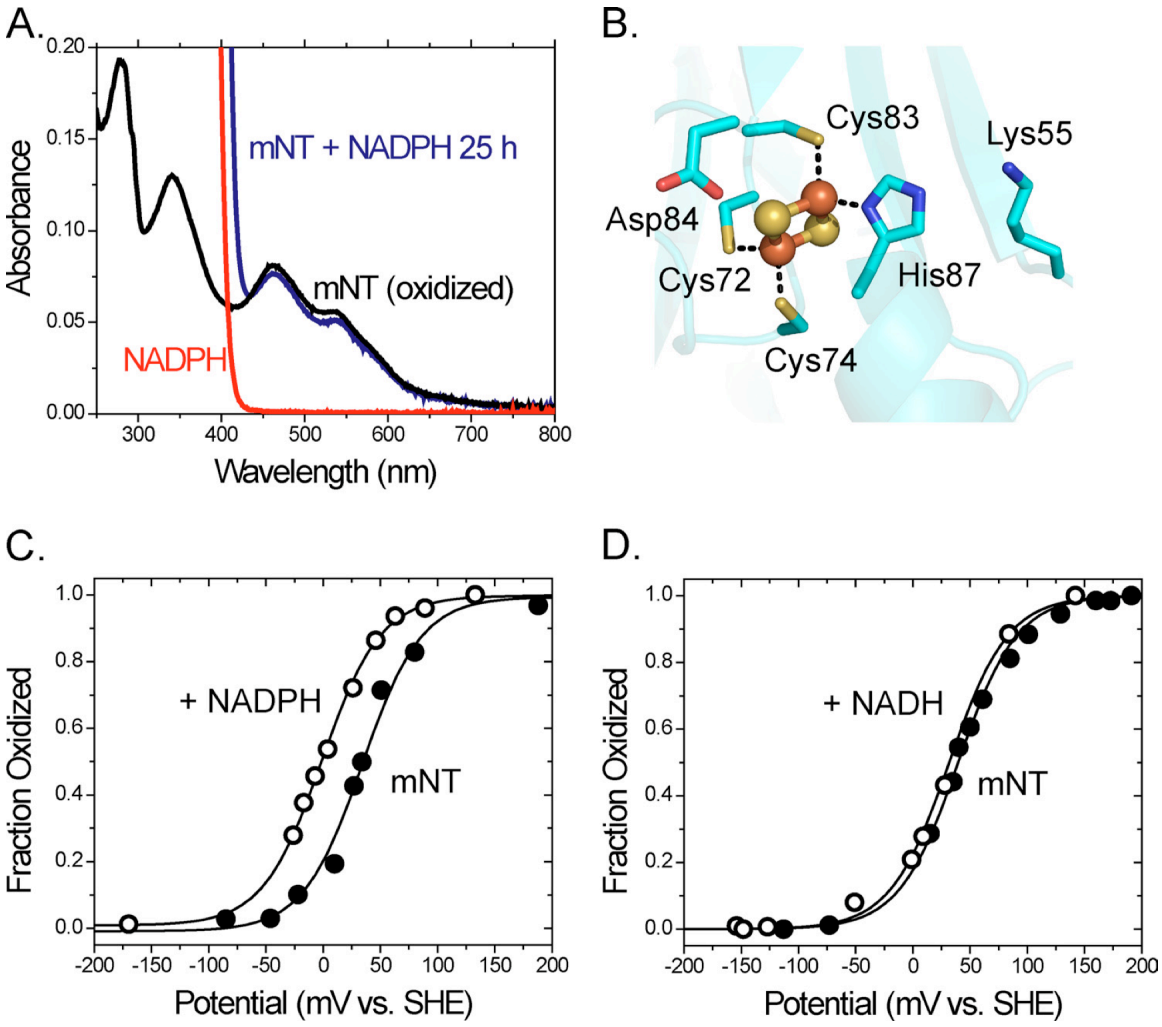

Figure 5-3: Optical potentiometric titrations in the presence of NADPH lead to changes in redox properties of mNT. A, visible spectrum of mNT (black line). Addition of NADPH in the absence of mediators does not reduce mNT even after 25 h (blue line). Visible spectrum of NADPH (red line) shows that there is no overlap at 458 nm where mNT has a λ_{max} that is used for monitoring the [2Fe-2S] cluster. B, directly coordinating ligands: Cys72, Cys74, Cys83, and His-87 as well as cluster-interacting residue Asp84. C and D, redox potential of mNT measured by titrating dithionite into a solution of oxidized mNT (50 μM) with or without 10 mM NADPH or NADH in the presence of 100 mM BisTris, 100 mM NaCl, pH 6.0, and mediators (30).

Accelerated [2Fe-2S] Cluster Loss as Result of NADPH Binding in Ferredoxin-like 4-Cys mNT Mutant (H87C). The single coordinating histidine, His87, is critical for [2Fe-2S] cluster stability (47), cluster transfer (29), and redox properties (28). These cluster properties in the mutant protein are intriguing in light of the fact that the H87C mutant maintains a structure nearly identical to that of the WT protein (47) (Figure 5-5A). Accelerated loss of the [2Fe-2S] cluster by NADPH ($t_{1/2}$ = 700 min) was still observed in the H87C mutant ($t_{1/2}$ = 2200 min H87C alone) (Figure 5-5B) despite the fact that optical potentiometric titrations on the H87C mutant show no redox changes in the presence of 10 mM NADPH (Figure 5-5C). Taken together, the results suggest that His87 is partly responsible for the observed pK_{ox} shift induced by NADPH binding in WT mNT, yet this strictly conserved residue is not essential for binding to NADPH and accelerating cluster loss.

[2Fe-2S] Cluster-interacting Residue Asp84 in CDGSH Domain Is Necessary for Inhibition of [2Fe-2S] Cluster Transfer by NADPH. The next residue to examine in the CDGSH cluster binding region is the strictly conserved Asp84, which is within hydrogen bond distance of one of the sulfurs in the [2Fe-2S] cluster but invisible in previous NMR studies. Replacement of conserved Asp84 with Ser resulted in no accelerated cluster loss at pH 6.0 in the presence of NADPH ($t_{1/2}$ = 10 min in both cases) (Figure 5-6, black and white circles). To determine whether the natural decay of the cluster in the D84S mutant at pH 6.0 is significantly faster than any accelerated cluster loss induced by NADPH binding, the experiment was performed at pH 7.5, where the [2Fe-2S] cluster is an order of magnitude more stable in the D84S mutant.

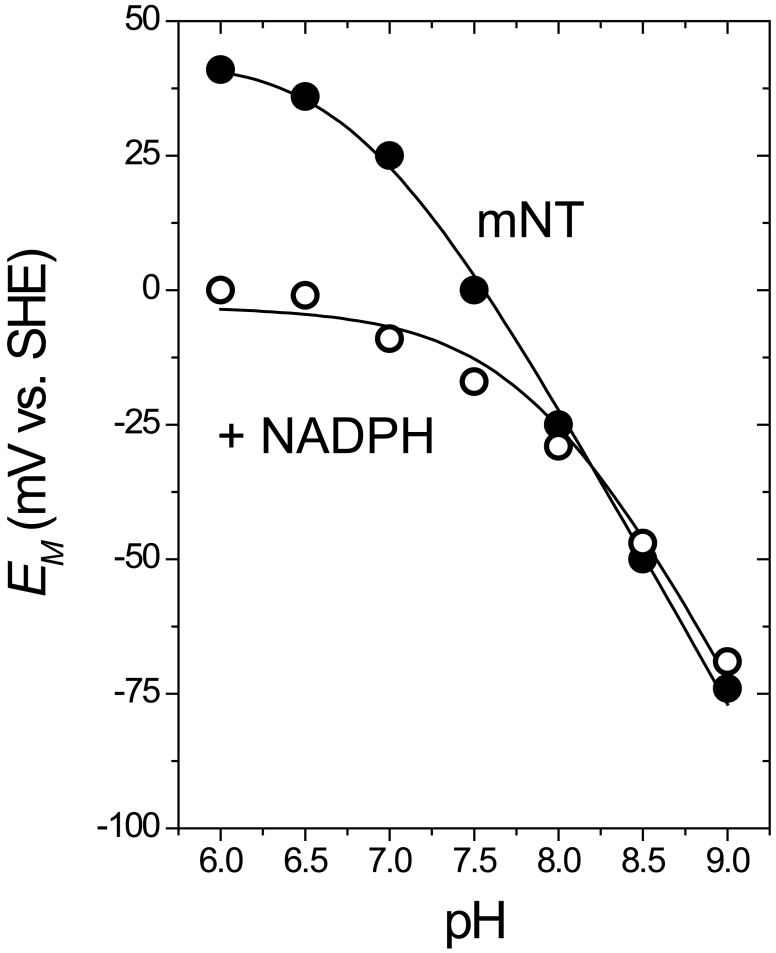

Figure 5-4: Binding of NADPH shifts redox properties (E_{acid} and pKox) of [2Fe-2S] cluster. In the presence of 10mM NADPH, E_{acid} drops from ~40 mV (28) to ~0 mV. In addition, pK_{ox} changes from 6.8 (43) to 7.8. Experiments were performed at 25 °C with and without 10mM NADPH using 50 μM mNT in 50 mM Bis-Tris, 50 mM Tris, 100 mM NaCl at varying pH in the presence of mediators (30).

No increased cluster loss of the D84S mutant by NADPH ($t_{1/2}$ = 1000 min in both cases) was observed (Figure 5-6A, black and white triangles). Having observed that the D84S mutant was no longer destabilized in the presence of NADPH, we decided to test whether cluster transfer was inhibited for the D84S mutant in the presence of NADPH. Replacement of Asp84 with Ser likely decreases the binding affinity of mNT for NADPH because cluster transfer was not noticeably inhibited (Figure 5-6B) even at 10 mM NADPH, which is significantly higher than physiological concentrations (~200 μM).

Our examination of the CDGSH cluster binding domain of this [2Fe-2S] protein implicated in type 2 diabetes using optical methods shows that the strictly conserved cluster-interacting residue Asp84 plays a direct role in NADPH binding and inhibition of [2Fe-2S] cluster transfer. Taken together, our results show that NADPH binding alters cluster stability and cluster transfer properties in this protein, and this likely has physiological consequences.

DISCUSSION

The recent discovery that NADPH binds to mNT and affects the stability of the [2Fe-2S] cluster led us to investigate whether the redox and cluster transfer properties of mNT are perturbed by interaction with this ubiquitous cofactor. The NMR methods previously showed specific residues that interact with NADPH, but the technical limitation of the paramagnetic broadening NMR technology imposed the difficulty of observing chemical shifts for residues in close proximity to the paramagnetic [2Fe-2S] cluster, specifically regarding the conserved CDGSH residues Asp84 and His87. The latter left open the possibility that residues in this region could be critical for facilitating

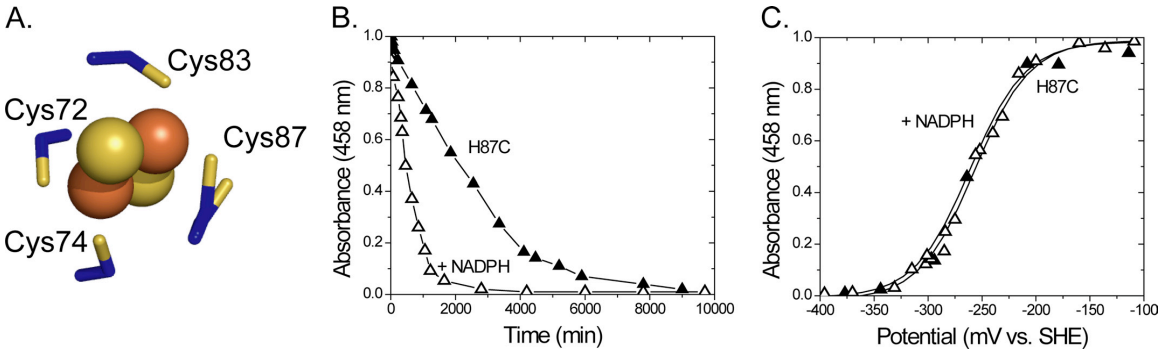

Figure 5-5: NADPH binding leads to accelerated cluster loss in 4-Cys mNT (H87C) in the absence of a redox shift. A, structure of H87C mutant (PDB entry 3LPQ) showing its 4-Cys coordination (47). Cys87 is found in two conformations in the crystal structure, and both conformations are shown (35). B, optical decay experiments showing time-dependent decrease in absorbance at 458 nm, indicating loss of [2Fe-2S] cluster for H87C mutant in the presence (black triangles) and absence of NADPH (white triangles). C, redox measurements show no shift in redox potential at pH 6.0 in the presence (black triangles) and absence of NADPH (white triangles). Decay experiments were performed at 35 °C atpH 6.0 using 50 μM H87C mutant with and without 10 mM NADPH in 100 mM Bis-Tris, 100 mM NaCl. Redox experiments were performed under similar conditions but at 25 °C (30).

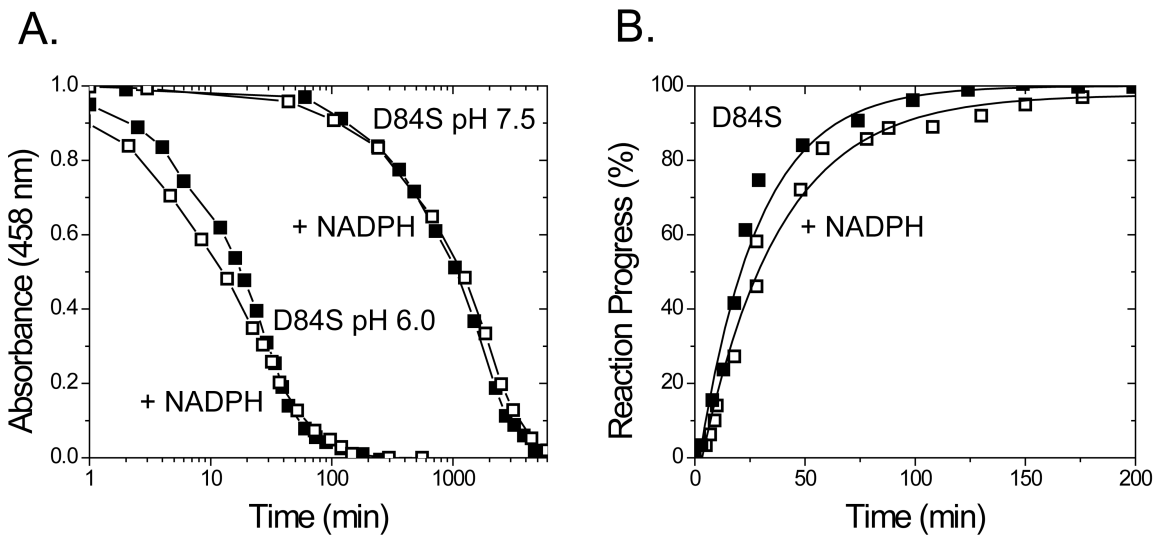

Figure 5-6: Asp84 is necessary for inhibition of [2Fe-2S] cluster transfer and accelerated cluster loss by NADPH. A, replacement of Asp84 with Ser (D84S) prevents accelerated loss of the cluster in the presence of NADPH. Experiments were performed at 35 °C at pH 6.0 (black and white squares) or 7.5 (black and white squares) using 50 μM protein with or without 10 mM NADPH in the presence of 100 mM Bis-Tris, 100 mM NaCl. B, transfer of [2Fe-2S] cluster from D84S mutant to a-Fd in the presence (white squares) and absence (black squares) of 10mM NADPH. Transfer experiments were performed using 100 μM D84S mutant and 100 μM a-Fd in 50 mM Bis-Tris, 100 mM NaCl with and without 10 mM NADPH (30).

both NADPH binding and the corresponding effects on cluster properties, e.g. cluster stability, cluster redox potential, and cluster transfer. Our investigation led us to the discovery that binding of NADPH to mNT inhibits the [2Fe-2S] cluster from being transferred to a-Fd (Figure 5-2B). This inhibition occurs even though the [2Fe-2S] cluster in mNT is oxidized in these experiments, when transfer is expected to occur readily. In addition, the conserved Asp84 in the CDGSH domain of the protein is critical for inhibition of [2Fe-2S] cluster transfer by NADPH.

A functional role for Asp84 in the binding of NADPH may explain why this residue is highly conserved through evolution and in all CDGSH proteins. Because NADPH plays a very important functional role in providing strong reducing equivalents in the cytosolic environment of all organisms, the inhibition of [2Fe-2S] cluster transfer in mNT at physiological concentrations of ~200 μM (Figure 5-2B) suggests a functional importance to this binding interaction and the likely necessity of this aspartyl group over the course of evolution. It is likely no accident that this conserved aspartyl group is positioned potentially to interact with both the sulfur moiety of the [2Fe-2S] cluster as well as a hydrogen bond donor on NADPH.

Our findings led us to propose an additional dimension to our understanding of the physiological role of [2Fe-2S] cluster transfer in mNT and how the protein behaves in patients with type 2 diabetes (29). We propose that NADPH acts as a regulator of mNT [2Fe-2S] cluster transfer, whereby it not only prevents transfer of the [2Fe-2S] cluster to acceptor proteins or into the mitochondrial matrix, but also accelerates loss of the [2Fe-2S] cluster. The latter may be a means of down-regulating the protein under normal reducing conditions (Figure 5-7). Our model proposes that under normal cytosolic

conditions, i.e. reducing environment (38), mNT is incapable of cluster transfer and accumulation of Fe in the mitochondria is abrogated. If NADPH levels are dramatically decreased, such as under conditions of oxidative stress, NADPH is no longer available to prevent [2Fe-2S] cluster transfer to apo-acceptor proteins, nor is it able to down-regulate the protein. In this case iron accumulation occurs in the mitochondria, which is often observed in patients with type 2 diabetes (84, 85), and such a phenomenon is believed to damage cells, especially those that produce insulin (86-88). TZDs may act therapeutically by imitating the normal [2Fe-2S] cluster transfer inhibitory effects of NADPH. This view is supported by the fact that both NADPH and the TZDs cause an alkaline shift in pK_{ox} through either direct or indirect interactions with cluster-binding residue His87 (28). A complete understanding of the role of NADPH association with members of the CGDSH family still remains to be understood. Specifically, whether NADPH binding shows similar effects on the CDGSH family member, Miner1, whose up-regulation leads to greater longevity in mice (27) but whose missplicing of the Miner1 gene, CISD2 , leads to a rare but serious human disease known as Wolfram syndrome 2 (23). Determining whether NADPH inhibits cluster transfer in Miner1 is of high priority, as is determining whether NADPH can disrupt or enhance binding of Miner1 to anti-autophagic/anti-apoptotic proteins in the Bcl-2 family (54).

We show that NADPH inhibits cluster transfer at physiological concentrations of the coenzyme. Our findings indicate that NADPH, which was previously shown to interact with the protein and accelerate loss of the [2Fe-2S] cluster, also affects a functional property of the protein: [2Fe-2S] cluster transfer to apo-acceptor proteins. We here propose a likely physiological role for the mNT-NADPH interaction, which is to

prevent cluster transfer regardless of the [2Fe2S] oxidization state and to down-regulate the protein under normal reducing conditions.

Chapter 5, in part, is a reprint of the material as it appears in the Journal of Biological Chemistry by Zuris JA, Ali SS, Yeh H, Nguyen TA, Nechushtai R, Paddock ML, Jennings PA. 287 2012. The dissertation/thesis author was the primary investigator and author of this paper.

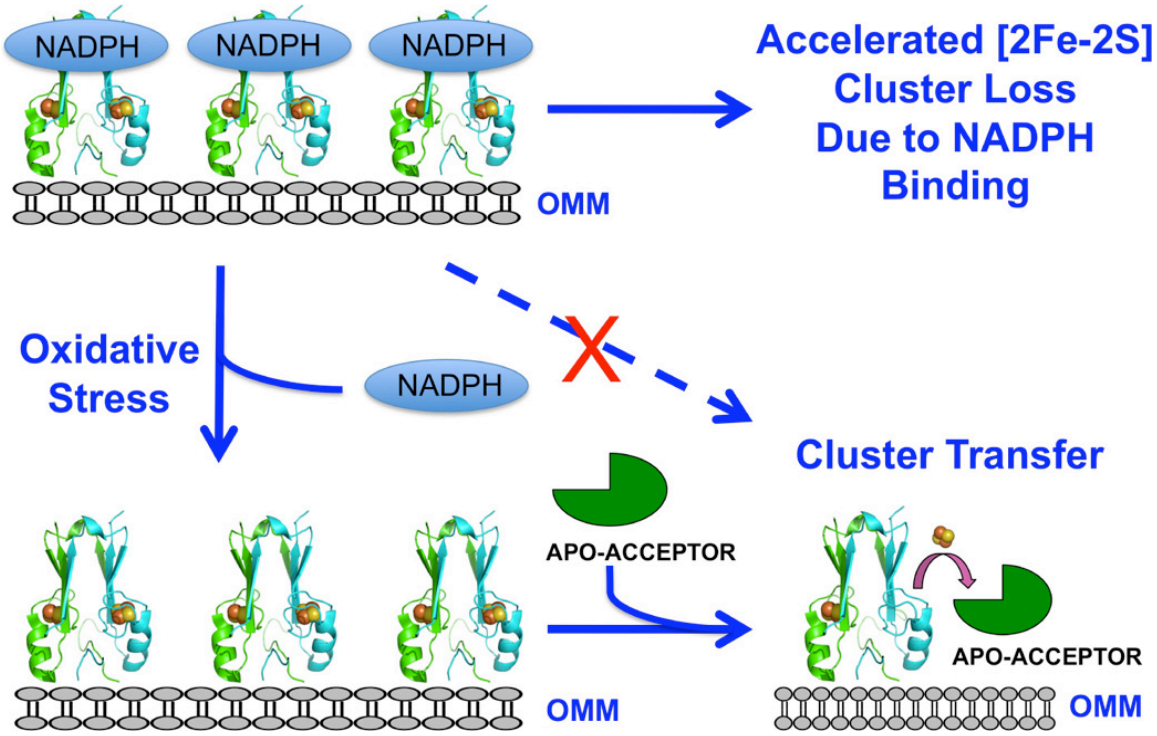

Figure 5-7: Model for NADPH regulation of mNT stability and cluster transfer properties. Under nominal conditions, NADPH inhibits [2Fe-2S] cluster transfer from mNT to an apo-acceptor protein and also causes accelerated loss of the [2Fe-2S] cluster in mNT. This provides two different means to regulate the activity of the protein under normal cellular conditions. However, when the cell experiences oxidative stress, mNT [2Fe-2S] clusters become oxidized and thus capable of [2Fe-2S] cluster transfer. As oxidative stress also leads to a decrease in NADPH levels (89), the inhibitory effect of NADPH on cluster transfer is alleviated and transfer can proceed (30).

Chapter 6

Future Directions: Characterization of the Interaction between MitoNEET and Voltage-Dependent Anion Channel (VDAC)

The integral membrane protein Voltage-Dependent Anion Channel (VDAC) is the most abundant outer-mitochondrial membrane (OMM) protein (90) and forms the primary path for diffusion of metabolites between the mitochondrial intermembrane space and the cytosol. VDAC is conserved across eukaryotes, with about 30% sequence identity between yeast and human. The three-dimensional structure of VDAC-1 reconstituted in LDAO micelles was solved by solution NMR (91). VDAC forms a large, 19-stranded β-barrel, which provides a pore for metabolite diffusion across the OMM. Electrophysiological experiments show that at low membrane potentials VDAC is in an open state, but it switches to the closed state at membrane potentials above 30 mV (92). However, the mechanistic details of this voltage gating process are not well understood. Because VDAC is involved in mitochondrial apoptotic pathways (93, 94), there is high interest in understanding its biological function and its binding partners. VDAC can interact with anti-apoptotic proteins from the Bcl-2 family, prohibiting the opening of the mitochondrial exit channel that leads to cell death (95). Other interaction partners of VDAC include the proteins hexokinase and the metabolites NADH and cholesterol (90, 91).

We postulate that mitoNEET (mNT) may transfer its [2Fe-2S} cluster into mitochondria via the VDAC channel (Figure 6-1). Based on mNT's β-cap width of ~15 Å and the VDAC pore size of 34 Å, there seems to be a potential fit for mNT, which hypothetically could remain tethered the OMM while protruding into the VDAC pore. Following a standard VDAC purification protocol, we tested whether VDAC affects mNT cluster stability in the presence of lipids (Figure 6-2A). We found that mNT is significantly destabilized by VDAC, suggesting that VDAC may act as a means of

transferring mNT [2Fe-2S] clusters into the mitochondria as we have observed in our RPA cellular assay (29). Furthermore, because we had not observed iron accumulation in the mitochondria with the 4-Cys mutant (H87C), we though that this would be a good control. We observed significant destabilization of the H87C mutant, though no destabilization for over 100 minutes (Figure 6-2B), which is longer than the RPA assay measurements. Therefore, our results with VDAC are consistent with the RPA cell assays and allow us to move further in our investigation. We plan to test whether pioglitazone can abrogate cluster destabilization of mNT in the presence of VDAC. We also will examine mNT-VDAC interactions by NMR and verify the importance of key contacts we see using a combination of point mutagenesis and decay/cluster transfer assays. Additionally, because VDAC is known to interact with NADH/NADPH (90), we plan to investigate whether similar mNT destabilization occurs in the presence of both VDAC and NADPH.

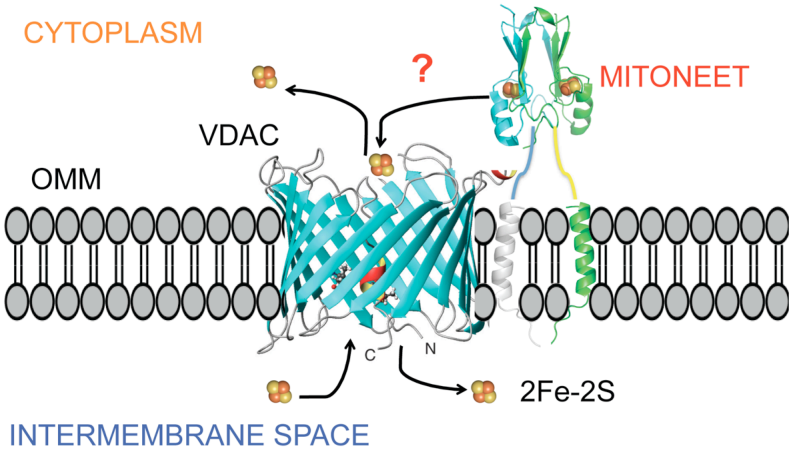

Figure 6-1: Proposed mechanism of mNT-VDAC interaction. We propose that mNT is able to transfer its cluster through the channel in VDAC channel as a mechanism to explain the observed iron accumulation in mitochondria (29) by oxidized mNT. VDAC NMR structure solved by Hiller et al. (91) is shown next to membrane-tethered mNT. We hypothesize that mNT can transfer its cluster into mitochondria by protruding into the VDAC channel.

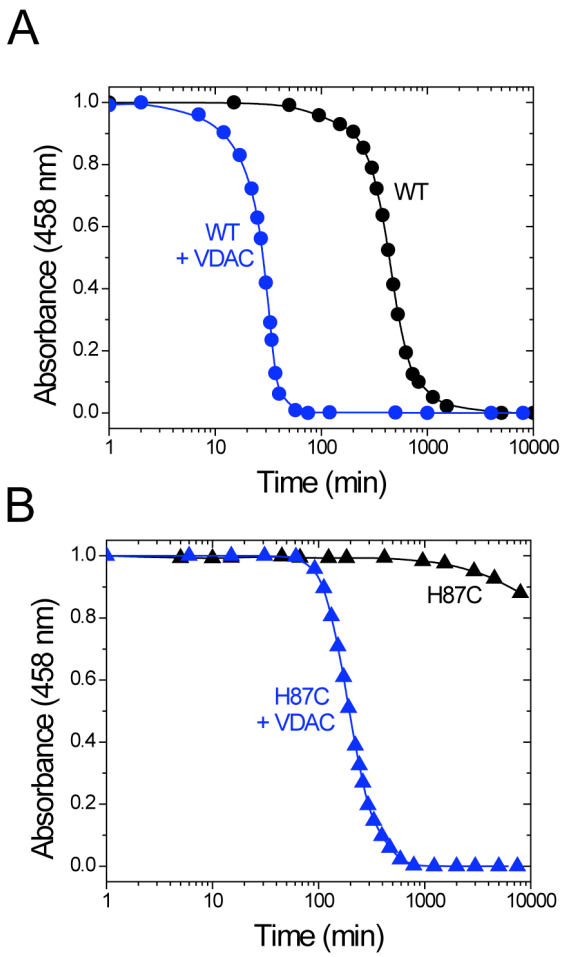

Figure 6-2: Both WT mNT and the H87C mutant are destabilized by VDAC. A) 50 μM WT mNT with (blue circles) and without 50 μM VDAC (black circles) in pH 6.5 Bis-tris 100 mM NaCl 0.1% LDAO. B) Replacement of single-coordinating His87 with Cys (H87C) stabilizes against cluster loss in the presence (blue triangles) and absence (black circles) of 50 μM VDAC. The H87C mutant is more stable than WT in the presence of VDAC.

References

1. Mokdad AH, Bowman BA, Ford ES, Vinicor F, Marks JS, & Koplan JP (2001) *JAMA* **286,** 1195-1200.

2. Reaven GM (1988) *Diabetes* **37,** 1595-1607.

3. Cheal KL, Abbasi F, Lamendola C, McLaughlin T, Reaven GM, & Ford ES (2004) *Diabetes* **53,** 1195-1200.

4. Chang AY, Wyse BM, Gilchrist BJ, Peterson T, & Diani AR (1983) *Diabetes* **32,** 830-838.

5. Sohda T, Meguro K, & Kawamatsu Y (1984) *Chem Pharm Bull (Tokyo)* **32,** 2267-2278.

6. Olefsky JM & Saltiel AR (2000) *Trends Endocrinol Metab* **11,** 362-368.

7. Pittas AG & Greenberg AS (2002) *Expert Opin Pharmacother* **3,** 529-540.

8. Norris AW, Chen L, Fisher SJ, Szanto I, Ristow M, Jozsi AC, Hirshman MF, Rosen ED, Goodyear LJ, Gonzalez FJ*, et al.* (2003) *J Clin Invest* **112,** 608-618.

9. Colca JR, McDonald WG, Waldon DJ, Leone JW, Lull JM, Bannow CA, Lund ET, & Mathews WR (2004) *Am J Physiol Endocrinol Metab* **286,** E252-260.

10. Wiley SE, Paddock ML, Abresch EC, Gross L, van der Geer P, Nechushtai R, Murphy AN, Jennings PA, & Dixon JE (2007) *J Biol Chem* **282,** 23745-23749.

11. Wiley SE, Murphy AN, Ross SA, van der Geer P, & Dixon JE (2007) *Proc Natl Acad Sci U S A* **104,** 5318-5323.

12. Paddock ML, Wiley SE, Axelrod HL, Cohen AE, Roy M, Abresch EC, Capraro D, Murphy AN, Nechushtai R, Dixon JE*, et al.* (2007) *Proc Natl Acad Sci U S A* **104,** 14342-14347.

13. Hou X, Liu R, Ross S, Smart EJ, Zhu H, & Gong W (2007) *J Biol Chem* **282,** 33242-33246.

14. Lin J, Zhou T, Ye K, & Wang J (2007) *Proc Natl Acad Sci U S A* **104,** 14640-14645.

15. Bian S & Cowan JA (1999) *Coordination Chemistry Reviews* **190-192,** 1049-1066.

16. Meyer J (2008) *J Biol Inorg Chem* **13,** 157-170.

17. Lill R & Muhlenhoff U (2008) *Annu Rev Biochem* **77,** 669-700.

18. Bandyopadhyay S, Chandramouli K, & Johnson MK (2008) *Biochem Soc Trans* **36,** 1112-1119.

19. Beinert H, Holm RH, & Munck E (1997) *Science* **277,** 653-659.

20. Fontecave M (2006) *Nat Chem Biol* **2,** 171-174.

21. Rouault TA & Tong WH (2008) *Trends Genet* **24,** 398-407.

22. Sheftel A, Stehling O, & Lill R (2010) *Trends Endocrinol Metab* **21,** 302-314.

23. Amr S, Heisey C, Zhang M, Xia XJ, Shows KH, Ajlouni K, Pandya A, Satin LS, El-Shanti H, & Shiang R (2007) *Am J Hum Genet* **81,** 673-683.

24. Barrett TG & Bundey SE (1997) *J Med Genet* **34,** 838-841.

25. Barrett TG, Bundey SE, Fielder AR, & Good PA (1997) *Eye (Lond)* **11 (Pt 6),** 882-888.

26. Chen YF, Kao CH, Kirby R, & Tsai TF (2009) *Autophagy* **5,** 1043-1045.

27. Chen YF, Wu CY, Kirby R, Kao CH, & Tsai TF (2010) *Ann N Y Acad Sci* **1201,** 58-64.

28. Bak DW, Zuris JA, Paddock ML, Jennings PA, & Elliott SJ (2009) *Biochemistry* **48,** 10193-10195.

29. Zuris JA, Harir Y, Conlan AR, Shvartsman M, Michaeli D, Tamir S, Paddock ML, Onuchic JN, Mittler R, Cabantchik ZI*, et al.* (2011) *Proc Natl Acad Sci U S A* **108,** 13047-13052.

30. Zuris JA, Ali SS, Yeh H, Nguyen TA, Nechushtai R, Paddock ML, & Jennings PA (2012) *J Biol Chem* **287,** 11649-11655.

31. Mehta JL, Rasouli N, Sinha AK, & Molavi B (2006) *Int J Biochem Cell Biol* **38,** 794-803.

32. Feinstein DL, Spagnolo A, Akar C, Weinberg G, Murphy P, Gavrilyuk V, & Dello Russo C (2005) *Biochem Pharmacol* **70,** 177-188.

33. Lowell BB & Shulman GI (2005) *Science* **307,** 384-387.

34. Zu Y, Couture MM, Kolling DR, Crofts AR, Eltis LD, Fee JA, & Hirst J (2003) *Biochemistry* **42,** 12400-12408.

35. Schwarzer C, Illek B, Suh JH, Remington SJ, Fischer H, & Machen TE (2007) *Free Radic Biol Med* **43,** 300-316.

36. Marshall NM, Garner DK, Wilson TD, Gao YG, Robinson H, Nilges MJ, & Lu Y (2009) *Nature* **462,** 113-116.

37. Miller AF (2008) *Acc Chem Res* **41,** 501-510.

38. Martinovich GG, Cherenkevich SN, & Sauer H (2005) *Eur Biophys J* **34,** 937-942.

39. Conlan AR, Axelrod HL, Cohen AE, Abresch EC, Zuris J, Yee D, Nechushtai R, Jennings PA, & Paddock ML (2009) *J Mol Biol* **392,** 143-153.

40. Dutton PL (1978) *Methods Enzymol* **54,** 411-435.

41. Leger C, Elliott SJ, Hoke KR, Jeuken LJ, Jones AK, & Armstrong FA (2003) *Biochemistry* **42,** 8653-8662.

42. Hirst J (2006) *Biochim Biophys Acta* **1757,** 225-239.

43. Zuris JA, Halim DA, Conlan AR, Abresch EC, Nechushtai R, Paddock ML, & Jennings PA (2010) *J Am Chem Soc* **132,** 13120-13122.

44. Dicus MM, Conlan A, Nechushtai R, Jennings PA, Paddock ML, Britt RD, & Stoll S (2010) *J Am Chem Soc* **132,** 2037-2049.

45. Iwasaki T, Samoilova RI, Kounosu A, Ohmori D, & Dikanov SA (2009) *J Am Chem Soc* **131,** 13659-13667.

46. Kuila D & Fee JA (1986) *J Biol Chem* **261,** 2768-2771.

47. Conlan AR, Paddock ML, Homer C, Axelrod HL, Cohen AE, Abresch EC, Zuris JA, Nechushtai R, & Jennings PA (2011) *Acta Crystallogr D Biol Crystallogr* **67,** 516-523.

48. Klingen AR & Ullmann GM (2004) *Biochemistry* **43,** 12383-12389.

49. Denke E, Merbitz-Zahradnik T, Hatzfeld OM, Snyder CH, Link TA, & Trumpower BL (1998) *J Biol Chem* **273,** 9085-9093.

50. Colca JR & Kletzien RF (2006) *Expert Opin Investig Drugs* **15,** 205-210.

51. Hofmann CA & Colca JR (1992) *Diabetes Care* **15,** 1075-1078.

52. Cavender MA, Nicholls SJ, & Lincoff AM (2010) *Eur J Cardiovasc Prev Rehabil* **17 Suppl 1,** S32-37.

53. Schmidt MV, Brune B, & von Knethen A (2010) *ScientificWorldJournal* **10,** 2181-2197.

54. Chang NC, Nguyen M, Germain M, & Shore GC (2010) *EMBO J* **29,** 606-618.

55. Johnson DC, Dean DR, Smith AD, & Johnson MK (2005) *Annu Rev Biochem* **74,** 247-281.

56. Adinolfi S, Iannuzzi C, Prischi F, Pastore C, Iametti S, Martin SR, Bonomi F, & Pastore A (2009) *Nat Struct Mol Biol* **16,** 390-396.

57. Napier I, Ponka P, & Richardson DR (2005) *Blood* **105,** 1867-1874.

58. Camaschella C, Campanella A, De Falco L, Boschetto L, Merlini R, Silvestri L, Levi S, & Iolascon A (2007) *Blood* **110,** 1353-1358.

59. Sohn YS, Breuer W, Munnich A, & Cabantchik ZI (2008) *Blood* **111,** 1690-1699.

60. Hausmann A, Samans B, Lill R, & Muhlenhoff U (2008) *J Biol Chem* **283,** 8318-8330.

61. Hentze MW, Muckenthaler MU, & Andrews NC (2004) *Cell* **117,** 285-297.

62. Hansen TM & Nagley P (2003) *Sci STKE* **2003,** PE31.

63. Cusimano EM, Knight AR, Slusser JG, Clancy RL, & Pierce JD (2009) *Adv Emerg Nurs J* **31,** 54-62.

64. Abdul-Ghani MA & DeFronzo RA (2008) *Curr Diab Rep* **8,** 173-178.

65. Baxter EL, Jennings PA, & Onuchic JN (2011) *Proc Natl Acad Sci U S A* **108,** 5266-5271.

66. Tirrell TF, Paddock ML, Conlan AR, Smoll EJ, Jr., Nechushtai R, Jennings PA, & Kim JE (2009) *Biochemistry* **48,** 4747-4752.

67. Petrat F, Weisheit D, Lensen M, de Groot H, Sustmann R, & Rauen U (2002) *Biochem J* **362,** 137-147.

68. Rauen U, Kerkweg U, Weisheit D, Petrat F, Sustmann R, & de Groot H (2003) *Free Radic Biol Med* **35,** 1664-1678.

69. Fish A, Danieli T, Ohad I, Nechushtai R, & Livnah O (2005) *J Mol Biol* **350,** 599-608.

70. Peter GF & Thornber JP (1991) *J Biol Chem* **266,** 16745-16754.

71. Glickstein H, El RB, Shvartsman M, & Cabantchik ZI (2005) *Blood* **106,** 3242-3250.

72. Nishikawa M, Nojima S, Akiyama T, Sankawa U, & Inoue K (1984) *J Biochem* **96,** 1231-1239.

73. Glickstein H, El RB, Link G, Breuer W, Konijn AM, Hershko C, Nick H, & Cabantchik ZI (2006) *Blood* **108,** 3195-3203.

74. Esposito BP, Epsztejn S, Breuer W, & Cabantchik ZI (2002) *Anal Biochem* **304,** 1-18.

75. Abramoff M, Magalhaes P, & Ram S (2004) *Biophotonics Int* **11,** 36-42.

76. Wu SP, Wu G, Surerus KK, & Cowan JA (2002) *Biochemistry* **41,** 8876-8885.

77. Shimomura Y, Wada K, Fukuyama K, & Takahashi Y (2008) *J Mol Biol* **383,** 133-143.

78. Black PH (2003) *Brain Behav Immun* **17,** 350-364.

79. Netz DJ, Pierik AJ, Stumpfig M, Muhlenhoff U, & Lill R (2007) *Nat Chem Biol* **3,** 278-286.

80. Zhou T, Lin J, Feng Y, & Wang J (2010) *Biochemistry* **49,** 9604-9612.

81. Albe KR, Butler MH, & Wright BE (1990) *J Theor Biol* **143,** 163-195.

82. Andersen KB & von Meyenburg K (1977) *J Biol Chem* **252,** 4151-4156.

83. Baxter EL, Jennings PA, & Onuchic JN (2012) *Proc Natl Acad Sci U S A* **109,** 1955-1960.

84. Hernandez C, Genesca J, Ignasi Esteban J, Garcia L, & Simo R (2000) *Med Clin (Barc)* **115,** 21-22.

85. Jiang R, Manson JE, Meigs JB, Ma J, Rifai N, & Hu FB (2004) *JAMA* **291,** 711-717.

86. Opara EC (2004) *J Investig Med* **52,** 19-23.

87. Valko M, Morris H, & Cronin MT (2005) *Curr Med Chem* **12,** 1161-1208.

88. Wolff SP (1993) *Br Med Bull* **49,** 642-652.

89. Pollak N, Dolle C, & Ziegler M (2007) *Biochem J* **402,** 205-218.

90. Colombini M (2004) *Mol Cell Biochem* **256-257,** 107-115.

91. Hiller S, Garces RG, Malia TJ, Orekhov VY, Colombini M, & Wagner G (2008) *Science* **321,** 1206-1210.

92. Colombini M (1979) *Nature* **279,** 643-645.

93. Kroemer G, Galluzzi L, & Brenner C (2007) *Physiol Rev* **87,** 99-163.

94. Malia TJ & Wagner G (2007) *Biochemistry* **46,** 514-525.

95. Shimizu S, Narita M, & Tsujimoto Y (1999) *Nature* **399,** 483-487.